THERMAL EXPANSION OF TETRAHEDRALLY BONDED SOLIDS AT LOW TEMPERATURES

PAUL WHITNEY SPARKS

THERMAL EXPANSION OF TETRAHEDRALLY BONDED SOLIDS AT LOW TEMPERATURES

by

Paul Whitney Sparks

An Abstract of

A Dissertation Submitted to the

Graduate Faculty in Partial Fulfillment of

The Requirements for the Degree of

DOCTOR OF PHILOSOPHY

Approved:

_____
In Charge of Major Work

_____
Head of Major Department

_____
Dean of Graduate College

Iowa State University
Of Science and Technology
Ames, Iowa

1966

THERMAL EXPANSION OF TETRAHEDRALLY BONDED SOLIDS AT LOW TEMPERATURES

Paul Whitney Sparks

Under the supervision of C. A. Swenson
From the Department of Physics
Iowa State University of Science and Technology

The linear thermal expansions of Si, Ge, GaAs, GaSb, InAs, and InSb were measured between $2^{o}K$ and $30^{o}K$ using a linear variable transformer technique*. Sensitivities in length changes of 10 cm long samples of close to 0.02A^{o} were observed. In general, the data show a region of positive thermal expansion at very low temperatures and this is followed by a region of relatively large negative thermal expansion at higher temperatures. From previous work it is known that at still higher temperatures the thermal expansion again becomes positive. The present data on Ge and Si agree satisfactorily with previous results.

On a reduced plot, the features of the curves for the various solids, with the exception of Si, show a systematic dependence on θ_o. The meaning of these correlations and their lack of application to Si is not obvious from a theoretical standpoint. The values of γ_o, the low temperature limit of the Gruneisen constant, determined for Ge and Si (0.66 and 0.44 respectively) do not agree with those calculated from the pressure dependence of the elastic constants (0.50 and 0.25). This is well outside expected errors. For $T/\theta_o \leq 0.02$, the thermal expansion coefficients of all the samples

---

*USAEC Report IS-T-114. This work was performed under contract W-7405-eng-82 with the Atomic Energy Commission.

vary as T^3. This is surprising since the specific heat does not show a T^3 temperature dependence for Ge or Si except at much lower temperatures ($T/\theta_o < .01$). As a result, γ shows an initial decrease as the temperature increases.

THERMAL EXPANSION OF TETRAHEDRALLY BONDED SOLIDS AT LOW TEMPERATURES

by

Paul Whitney Sparks

A Dissertation Submitted to the
Graduate Faculty in Partial Fulfillment of
The Requirements for the Degree of
DOCTOR OF PHILOSOPHY

Major Subject: Physics

TABLE OF CONTENTS

	Page
INTRODUCTION	1
DISCUSSION OF APPARATUS	12
Sample Chamber and Sensing Coil	16
Dewar System	23
Heater Supply	26
Mutual Inductance Circuit	27
Thermometry	42
CALIBRATION	46
EXPERIMENTAL PROCEDURE	51
RESULTS	56
DISCUSSION OF RESULTS	79
CONCLUSIONS	90
LITERATURE CITED	92
ACKNOWLEDGMENTS	95
APPENDIX	96

INTRODUCTION

A solid consists of a system of particles in stable equilibrium which vibrate constantly with small amplitudes. The free energy,

$$F = U-TS, \tag{1}$$

of such a system is given by

$$F = -kT \ln Z, \tag{2}$$

where Z is the partition function. In such a system the lattice potential energy may be written as

$$\phi = 1/2 \sum_{i,j}^{3N} A_{ij} q_i q_j + \phi_o(V) \quad , \tag{3}$$

where the q's are vector coordinates and the A_{ij}'s are constants. Hence, the Hamiltonian may be written as

$$H = 1/2m \sum_{j=1}^{3N} P_j^2 + 1/2 \sum_{i,j}^{3N} A_{ij} q_i q_j + \phi_o(V) \quad , \tag{4}$$

where the P_j's are the momentum vectors and ϕ_o is the lattice cohesive energy. This has a quantum mechanical solution with eigenvalues of the form

$$\epsilon_i = (n + 1/2)\, h\nu_i + \epsilon_o \quad , \tag{5}$$

where n is any given integer, ν_i is the frequency of the ith mode, and ϵ_o is related to $\phi_o(V)$. Therefore, the partition function,

$$Z = \sum_i \exp\, (-\epsilon_i/kT) \quad , \tag{6}$$

may be written as

$$Z = \sum_{i=1}^{3N} \exp(-\epsilon_o/kT) \exp(-1/2h\nu_i/kT) \sum_{n=0}^{\infty} \exp(-nh\nu_i/kT)$$

$$= \prod_{i=1}^{3N} \exp(-E_o/kT) [1-\exp(-h\nu_i/kT)]^{-1} \quad , \tag{7}$$

where E_o is a function of volume and contains the zero point and cohesive lattice energies. Hence,

$$F = E_o(V) + kT \sum_{i=1}^{3N} \ln[1-\exp(-h\nu_i/kT)] \quad . \tag{8}$$

It is seen that this expression is of the form

$$F = E_o(V) + F^*(V,T) \quad , \tag{9}$$

where

$$F^*(V,T) = kT \Sigma_i f_i(\nu_i/T) \quad . \tag{10}$$

The quasi-harmonic approximation which involves the assumption that the ν_i's are a function of volume will be used here. From the definition of the free energy given above (equation 1) it is seen that

$$F^* = U^*-TS \quad , \tag{11}$$

and it is easily shown that

$$U^* = \left(\frac{\partial F^*/T}{\partial 1/T}\right)_V$$

$$= K \sum_i \frac{df_i}{d(\nu_i/T)} \nu_i \quad . \tag{12}$$

Similarly, the pressure, P, is given by

$$P = -\left(\frac{\partial F}{\partial V}\right)_T$$

$$= -\left(\frac{\partial E_o}{\partial V}\right)_T - \left(\frac{\partial F^*}{\partial V}\right)_T \quad . \tag{13}$$

A thermal pressure, P*, can be defined as

$$P^* = -\left(\frac{\partial F^*}{\partial V}\right)_T$$

$$= -kT \sum_i \left(\frac{\partial f_i}{\partial V}\right)_T$$

$$= -k \sum_i \frac{df_i}{d(\nu_i/T)} \frac{d\nu_i}{dV} \quad . \tag{14}$$

Equations (12) and (14) can be used to show that

$$U_i^* = k \frac{df_i}{d(\nu_i/T)} \nu_i \quad , \tag{15}$$

and

$$P_i^* = -k \frac{df_i}{d(\nu_i/T)} \frac{d\nu_i}{dV} \quad . \tag{16}$$

Hence,

$$P_i^* = -\frac{U_i^*}{\nu_i} \frac{d\nu_i}{dV}$$

$$= -\frac{U_i^*}{V} \frac{d \ln \nu_i}{d \ln V}$$

$$= \frac{U_i^*}{V} \gamma_i \quad , \tag{17}$$

where

$$\gamma_i = -\frac{d \ln \nu_i}{d \ln V} \quad . \tag{18}$$

The total pressure on the solid is given by

$$P = P_o(V) + P^*(V,T)$$

$$= P_o(V) + \sum_i P_i^*(V,T) \quad . \tag{19}$$

The volume thermal expansion coefficient, β, and the isothermal bulk modulus, B_T, are related by the identity

$$\beta B_T = \left(\frac{\partial P}{\partial T}\right)_V \quad . \tag{20}$$

However, from equations (17) and (19)

$$\left(\frac{\partial P}{\partial T}\right)_V = \left(\frac{\partial P^*}{\partial T}\right)_V$$

$$= \sum_i \frac{\gamma_i}{V} \left(\frac{\partial U_i^*}{\partial T}\right)_V$$

$$= \sum_i \frac{\gamma_i C_{vi}}{V} \quad , \tag{21}$$

where C_{vi} is the specific heat of the i^{th} mode. Therefore,

$$\beta = \sum_i \frac{\gamma_i C_{vi}}{B_T V} \quad , \tag{22}$$

or

$$\beta = \frac{\gamma C_v}{V B_T} \quad , \tag{23}$$

where the Gruneisen parameter, γ, is defined as

$$\gamma = \frac{\Sigma C_{vi}\gamma_i}{\Sigma C_{vi}} \quad . \tag{24}$$

Equation (23) is relevant only to the lattice contribution to the thermal expansion coefficient; however, if there are other contributions, F_k, to the free energy which are additive, one may write

$$F = \sum_k F_k^* (V,T) + \sum_k F_k(V) \quad . \tag{25}$$

From equation (13) it is seen that

$$\left(\frac{\partial P}{\partial T}\right)_V = -\left(\frac{\partial^2 F}{\partial V \partial T}\right)_{V,T} \quad , \tag{26}$$

and from equation (20)

$$\beta B_T = -\left(\frac{\partial^2 F}{\partial V \partial T}\right)_{V,T} \quad . \tag{27}$$

Therefore, individual contributions to the thermal expansion coefficient may be defined as

$$\sum_k \beta_k = -\frac{1}{B_T} \sum_k \left(\frac{\partial^2 F_k}{\partial V \partial T}\right)_{V,T} = \beta \quad , \tag{28}$$

where B_T is the total bulk modulus at the volume and temperature, V and T. In the present experiment it is believed that contributions other than those due to the thermal energy of the lattice are of little importance and the most emphasis will be placed on equation (23).

The Debye theory gives perhaps the most successful first order method for treating the thermal properties of solids. In this theory one considers a set of harmonic oscillators as in equation (8) and then makes an

approximation to sum over the 3N modes. The approximation is that there is no dispersion between the wave vectors and frequencies in the solid, i.e. the velocity of sound is constant in the crystal. There is also a maximum frequency, ν_m, such that no frequencies higher than this value occur in the solid. The Debye theory then predicts that the specific heat of a solid will be given by

$$C_v = 9R \left(\frac{T}{\theta_D}\right)^3 \int_0^{\theta_D/T} \frac{e^x}{(e^x-1)^2} x^4 \, dx \quad , \tag{29}$$

where $\theta_D = \frac{h\nu_m}{k}$ and is known as the Debye temperature. This approximation becomes very good at very low temperatures ($T<\theta_D/50$) since in this range there is no dispersion in a real solid. In this case the Debye theory predicts that

$$C_v = 234R \left(T/\theta_D\right)^3 \quad . \tag{30}$$

A fit between experimental data and theory is usually made by considering the Debye temperature to be a function of temperature and in many cases specific heat data are presented as a plot of θ_D versus temperature. The limiting low temperature value of θ_D is usually designated as θ_o.

From the definition of γ (equation 24) it is seen that at high temperatures ($T \gg \theta_D$)γ becomes constant since all modes have the classical value of the specific heat, $C_{vi} = k$, and

$$\gamma = \sum_i \frac{\gamma_i}{3N} \quad . \tag{31}$$

In the low temperature limit ($T < \theta_D/50$)γ again becomes constant since only continuum lattice vibrational states are excited and there is no change in the relative weighting factors of the various modes. It is seen from equation (30) that the C_{vk}'s are proportional to T^3 where the γ_k's are summed over the transverse and longitudinal acoustic modes so

$$\gamma = \frac{\Sigma \gamma_k A_k T^3}{\Sigma A_k T^3} = \frac{\Sigma \gamma_k A_k}{\Sigma A_k} = \text{const.}, \tag{32}$$

where the various A_k's and γ_k's are constants. This low temperature limit may be expressed as

$$\gamma_o = - \frac{d \ln \theta_o}{d \ln V} , \tag{33}$$

where θ_o is the value of the Debye temperature at $T = 0^oK$ and may be related to the pressure dependence of the elastic constants. There is no reason for these two limits of γ to be equal so the experimental γ is in general a function of temperature. For a typical solid such as NaCl the values of the high and low temperature limits of γ are 1.51 and 0.93 respectively (1).

At low temperatures, $(\theta_D/10)$, V, B_T, and γ are fairly constant so from equations (23) and (30) it is seen that

$$\beta \cong \text{const. } T^3 . \tag{34}$$

The thermal expansion coefficient of NaCl, for instance, is of the order of $10^{-10}T^3$. The present experiment, however, involves the thermal expansion coefficients of some diamond structure materials, for which the values of β will be almost two orders of magnitude smaller than this. This arises because of smaller γ's and relatively larger θ's of these materials. It is therefore necessary to detect a relative change in the size of a solid of the order of a few parts in 10^{11}.

Experimentally, the linear thermal expansion coefficient, $\alpha = \frac{1}{L_o} (\frac{\partial L}{\partial T})_p$, is measured and for a cubic material α is related to β by

$$\alpha = \beta/3 . \tag{35}$$

Experimental methods based on x-ray diffraction or optical interferometry

techniques do not have the sensitivity necessary to measure expansion coefficients as small as $10^{-8}/^{o}K$. Three very different types of apparatus have been developed which do have this sensitivity. First, a double grid arrangement has been used with one grid moving with respect to the other (2). The relative transmission of light through this combination is measured using a differential photocell, and results are quoted to a fraction of an $\mathring{A}$. A modification of the above principle which uses a tilting mirror to shift the optical image of one grid with respect to the other has been tried at room temperatures. The detection of sample movement of $10^{-4}\mathring{A}$ has been claimed (3), but this method has not been adapted to low temperature measurements.

A second method involves plating the top surface of a sample and using this surface as one plate of a variable capacitor in a bridge circuit (4). This method is one of the most sensitive now in use for measuring low temperature thermal expansion, and changes in length of a few tenths angstrom can be detected. The major limitation of this method involves the stability of the capacitor plates and the need for small plate separation.

The method used in the present work consists of using a linear variable transformer to measure the expansion of the sample (5). As the sample changes length the motion is transferred to the secondary coil of a linear variable transformer and is measured by the use of a mutual inductance bridge. Changes in length can be detected with a precision of $0.02\mathring{A}$ and a mean scatter of $\pm 0.02\mathring{A}$ is maintained where necessary over a range of one angstrom.

Prior to 1958 negative thermal expansions were observed in such solids

as silver iodide (6), silicon (7), vitreous silica (8), zinc blende (9), and α-uranium (10). This behavior in these materials is significant in that the negative thermal expansion is a result of their crystal structure and is strictly a lattice phenomenon. This is unlike magnetic materials such as invar where an additional magnetic term is added to the free energy to produce a net negative expansion. In 1958 Gibbons (11) measured the thermal expansion of Ge, Si, and InSb and found negative expansions for all of these materials at low temperatures. Following a suggestion due to Blackman (12) Gibbons concluded that negative γ_i's for these materials could result since all of these materials have fourfold coordination (tetrahedrally bonded), loosely packed structures, and are strongly covalent.

These measurements were extended by Novikova over the next few years in an extensive investigation of the thermal expansion of diamond structure materials from room temperatures to as low as $20^{\circ}K$. Si (13), Ge (14), and diamond (15) were measured first and the results confirmed those of Gibbons. The isoelectronic series, α-Sn, InSb, and CdTe (16); and GaAs, ZnSe (17) and Ge (14) were measured and it was found that the temperature at which α becomes negative increases as the value of α_{min} becomes smaller when passing from a group IV material to a group II-VI material. This led the author to conclude that "... this result corresponds to the increase of the strength of the ionic components of the bonds." (17). In 1963 Novikova measured the thermal expansions of AlSb, GaSb, ZnTe, and HgTe (18) with the same general results.

Carr, McCammon, and White (19) performed some very fine measurements on Ge and Si at lower temperatures ($6^{\circ}K$ to $100^{\circ}K$) with 0.5 angstrom sensitivity. This work demonstrated the presence of a region of positive

expansion in these two materials from $0^{o}K$ up to $T/\theta_{o} \approx 0.025$. The existence of this low temperature positive region had been suggested by Daniels (20) using equation (32) and taking a weighted average of the pressure derivatives of the elastic constants based upon the acoustic work of McSkimmin (21). The thermal expansion data were not sufficiently precise, however, to give the details of the positive region although the negative expansion region was investigated in some detail.

The most recent thermal expansion experimental work completed on diamond structure materials was again done by Novikova in a study of the effect of adding impurities to Ge (22) and Si (23). It was found that electronic impurities with a concentration greater than about $10^{17}/cm^{3}$ would increase by a few percent the absolute magnitude of the thermal expansion coefficient and the transition temperature where α became negative. The same behavior was shown to be given by a dislocation density of the order of $10^{7}/cm^{3}$. This further confirms some work done on active impurities in Ge by Keyes (24).

The theory of negative thermal expansions in general and that of diamond structures specifically has been studied for several years and although considerable insight has been achieved over this period there is unfortunately no complete theory to describe the details of this phenomenon. Blackman (12) demonstrated that a negative thermal expansion coefficient was feasible in both the sodium chloride and zinc blende structures. From this work the phenomenon of negative thermal expansion passed from being an abnormal behavior of materials to possibly the normal behavior for materials with a loosely packed structure.

As pointed out by Daniels (25) the existence of a region of negative

thermal expansion is not the only anomaly of these materials. At high temperatures the value of α is almost an order of magnitude lower than expected of most materials. Also the specific heats of these materials exhibit large minima in the value of θ_D at about $T = \theta_D/5$.

A more sophisticated model must be used to fit the existing data and Bienenstock (26) used a nearest-neighbor plus a dipole-dipole interaction model to make a one parameter fit to the experimental γ's of Ge. A successful fit was achieved, but it is difficult to assign any physical significance to the one parameter.

The purpose of this experiment is to investigate the low temperature thermal expansions of some diamond structure solids primarily in the low temperature region where their expansions are positive. It was hoped to determine if these materials behaved at very low temperatures as Debye solids ($\alpha = AT^3$) and if any correlations and explanations can be given for their behavior in the temperature region where their expansions become anomalous.

DISCUSSION OF APPARATUS

The apparatus in general is based on that described by Carr (5) with several major modifications which will be discussed below. Figure (1) is a schematic representation of the primary components of the equipment and their relationship to each other. This equipment may be divided into four basic systems: sample suspension, sample heating, sample expansion measurement, and thermometry. These systems must respectively support and isolate the sample from its ambient surroundings, vary the temperature of the entire sample uniformly above the ambient temperature, measure the change in length of the sample, and measure the temperature of the sample.

Polished sapphire disks are glued to both ends of the sample and to the base of the sample chamber. The disks at the bottom of the sample and at the base of the sample chamber are indented and a small sapphire ball is placed between them to provide a gimbal bearing. This bearing provides for the transverse support of the bottom of the sample and also corrects for small mistakes in alignment. Transverse support for the top of the sample is accomplished by attaching three nylon threads about one-fourth of the way down from the top of the sample, passing them over small pulleys, and attaching them to small springs.

At the top of the sample a fourth sapphire disk is glued to a copper strip which leads to the bath. When the sample is mounted this disk is in contact with the disk at the top of the sample and a quartz rod is placed between the copper strip, i.e. the top of the sample, and the secondary coil of the linear variable transformer expansion sensing device. Since there is a vacuum in the sample chamber, the polished surfaces of the disks provide

Figure 1. General electrical and mechanical schematic drawing of the thermal expansion measuring apparatus

THERMAL EXPANSION SCHEMATIC DRAWING

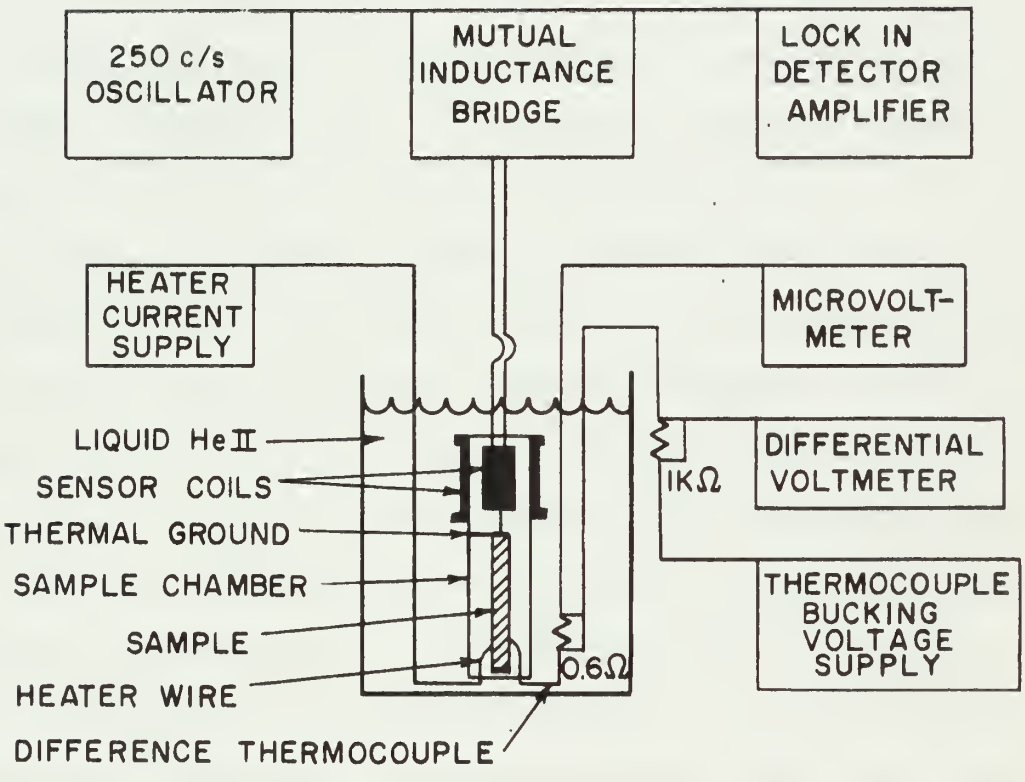

for a high thermal impedance and at the same time maintain good mechanical contact throughout the expansion system.

Sample heating is accomplished by passing a small current through a manganin wire heater which is wound on and glued to the sample. This heat will raise the temperature of the sample uniformly (if the thermal impedance of the sapphire disk junctions is much greater than that of the sample) until an equilibrium is reached where the heat delivered into the sample is equal to the heat loss through the ends of the sample into the bath.

A linear differential transformer is used to measure the sample expansion. The secondary coil is in mechanical contact with the sample by means of a quartz rod. The primary and secondary coils are wound in such a way that when an alternating current is passed through the primary coil a voltage is induced in the secondary coil which for small displacements from the center position is proportional to the change in position. This induced voltage is sensed as a change in the coupling between the primary and secondary coils and is measured using a mutual inductance bridge.

The temperature of the sample is measured with an Au-Fe versus Cu differential thermocouple (27). One junction of the thermocouple is attached to the sample and the other junction is in the helium bath. Since the bath temperature can be determined from vapor pressure readings (it is held at a constant temperature below the helium λ point with a large Cartesian manostat) the absolute temperature of the sample can be found directly from the thermocouple voltage, which is measured by a potentiometric method. A detailed discussion of the various equipment components will be given in the following sections.

Sample Chamber and Sensing Coil

Once the approximate size of the sample has been decided upon, four basic problems must be solved: a method for transmitting the motion of the sample to the secondary coil, a method for supporting the secondary coil, a method for supporting and insulating the sample from bath temperature, and a method for introducing the electrical leads into the sample chamber.

In this experiment the secondary coil is placed inside of the sample chamber and a direct mechanical linkage is provided between the sample and the secondary coil (see Figure 2). This method eliminates the need for a diaphragm as used by Carr (5). The use of a diaphragm allows the secondary coil to be placed directly in the helium bath so that it is maintained at a constant temperature. However, if a sample has a large thermal expansion, it will tend to pull away from the diaphragm upon cooling, while a sample with a small thermal expansion will tend to rupture the diaphragm upon cooling. The present method offers greater flexibility, at the expense of requiring rigorous thermal anchoring of the secondary.

The secondary coil is supported from a phenolic shield inside the sample chamber by three nylon threads glued to the top and bottom of the secondary coil and to the shield. The secondary coil is wound without a coil form and a quartz tube with one end sealed and indented is fixed axially within the coil. The quartz tube is glued with G.E. 7031 adhesive to the midpoint of the secondary coil since this minimizes the change in the balance point of the mutual inductance bridge upon cooling from room temperature to liquid helium temperatures. This also minimizes any effect due to extraneous heating. A 2mm quartz rod is glued to the sample thermal

Figure 2. Cutaway drawing of the sample chamber

SAMPLE CHAMBER

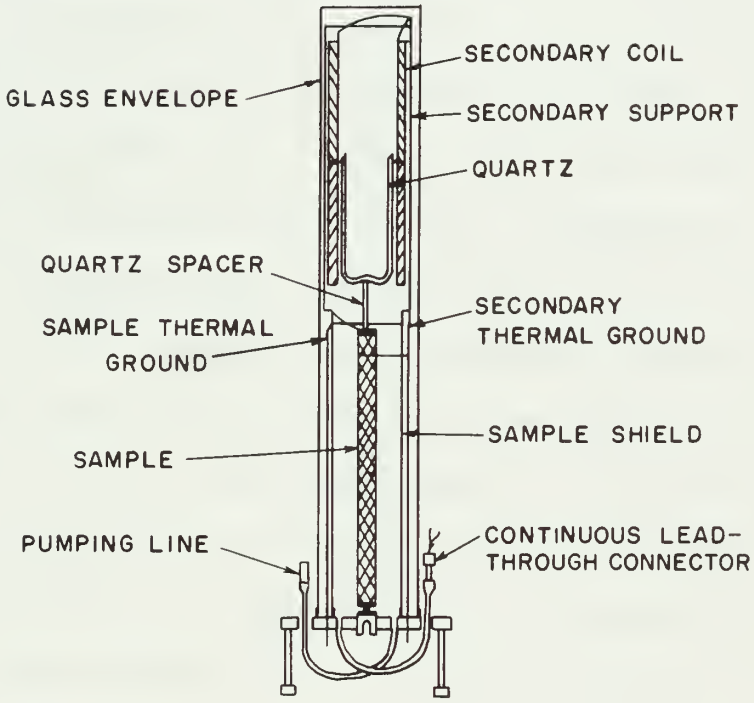

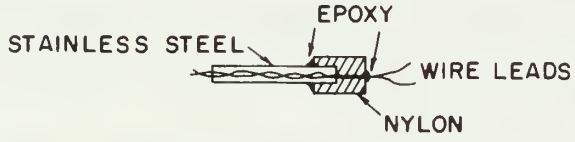

CONTINUOUS LEAD CONNECTOR

ground (copper strip) which is in direct mechanical contact with the sample. The other end of the rod is placed in the indentation in the quartz tube so that the secondary coil is connected to the sample.

This type of construction eliminates the use of a diaphragm and the associated loading problems, since the secondary coil is inside of the sample chamber. It is necessary, however, to insure that the temperature of the secondary coil stays extremely constant and close to the bath temperature, since heating of the secondary coil can affect the balance point through thermal expansion or susceptibility changes of the secondary coil. Since the secondary coil is in a vacuum in the sample chamber a mechanical heat conductance path to the bath is necessary to remove heat generated in the secondary coil by eddy currents. This is accomplished by placing three 0.002 in. copper strips longitudinally between the windings of the secondary coil, soldering them to another copper strip that leads down the phenolic shield in the sample chamber, and attaching this strip to a 0.06 in. copper rod which leads to the bath. To prevent heat from the sample from affecting the secondary coil, the sapphire disk at the top of the sample and the base of the quartz rod are attached to a sample thermal ground which consists of a 0.008 in. copper strip soldered to another copper rod which leads directly to the bath. In addition, a 0.01 in. copper wire is glued to the quartz spacer and to one of the copper rods. To check these precautions Fe-Au versus Cu differential thermocouples were temporarily installed on the secondary coil and on the sample thermal ground referenced to the base of the sample chamber. The tests were conducted with a primary current of 100 ma and a sample heater input of 20 milliwatts (sufficient to raise the sample temperature to about $30^{\circ}K$).

The temperature of the secondary coil rose 0.6°K due to eddy currents from the primary field and was unaffected by the sample heat. The temperature of the sample thermal ground rose 2°K due to the maximum sample heating power and was unaffected by the primary current. Calculations show that these values of heating of the secondary coil and sample thermal ground should produce effects that are two orders of magnitude less than the least count ($\pm$0.01Å) of the experiment.

As briefly described above the sample is supported and insulated through the use of sapphire disks and nylon threads. An important requirement in this experiment is that the thermal conduction of the sample be adequate to prevent thermal gradients from developing across the sample. If the thermal impedance provided by the sapphire disks is high, then less power can be used to elevate the temperature of the sample to the desired level and, therefore, there will be a smaller temperature gradient across the sample. In this experiment this condition is checked by comparing data taken with the complete heater in use with data taken with only one half of the heater in use (a center tap on the heater is provided for this purpose). If there are important thermal gradients in the sample these two sets of data will not agree.

A polished sapphire disk 1mm thick and 1/4 in. in diameter is glued to each end of the sample with G.E. 7031 adhesive. Another set of disks is glued to the base of the sample chamber and to the bottom of the sample thermal ground. If two hard polished surfaces are in contact in a vacuum a large thermal impedance is developed across the junction (28). Therefore these disks provide for a good thermal break and at the same time maintain mechanical continuity from the base of the sample chamber, through

the sample, along the quartz spacer, and to the secondary coil. The disks at the bottom of the sample and at the base of the sample chamber are indented and a 1mm sapphire ball is placed between them forming a gimbal bearing. This bearing provides transverse support for the base of the sample and also adjusts for small misalignments.

Three size A nylon threads are tied to the sample about one-quarter sample length from the top of the sample to provide transverse support for the top of the sample. These threads lead over small pulleys and are tied to springs constructed of spring bronze. The springs are attached to traveling screws so that after the threads are tied small adjustments may be made in the alignment of the sample. The pulleys and the traveling screws are glued and soldered respectively to a copper shield which surrounds the sample. This shield, which is made from 99.999% pure copper, is used both for sample support and for mounting the secondary phenolic shield.

With the incorporation of a thermocouple as the primary thermometer in the system, it became necessary to use a continuous-lead vacuum-tight connector to insure that thermoelectric voltages are not developed where the electrical leads leave the sample chamber. Hollow pin connectors, which were tried previously, were found to develop leaks a majority of the times that they were cooled to liquid nitrogen temperatures.

A connector was developed for this purpose (see Figure 2) by fitting a 1/8 in. stainless steel tube into a hole drilled in a 1/2 in. section of 3/8 in. diameter nylon rod. These two pieces are glued together with Armstrong A-4 epoxy adhesive after which a 1/32 in. hole is drilled in the nylon through which the wires are passed and glued. It is very important

that all surfaces including all of the wires are thoroughly cleaned and completely wetted with the glue before the joint is made. After the glue joints have been cured the wires are passed through a copper tube into the sample chamber and the stainless steel tube is soldered to a copper adapter with Wood's metal.

The remainder of the sample chamber consists of the glass envelope (1.75 in. O.D.) which has a 1.5 in. copper to glass feathered seal on one end and a piece of optical glass blown into the other end. This envelope is Wood's metalled to the base and the sample chamber is now vacuum-tight. The primary coil is placed over the outside of the glass envelope, is held transversely with two phosphor bronze springs, and is held longitudinally with a phenolic "cap". A screw which is in this cap pushes on the flat top of the glass envelope, and it is used to make gross adjustments (to about $\pm$0.1mm) in the balance point.

Since the sample lengths varied from 7 cm to 13.5 cm it was necessary to build two sample chambers. The first sample chamber was used for sample lengths of the order of 10 cm (although one sample was only 8.2 cm long) and was designed as described above and as shown in Figure 2. For the longer and shorter samples a second sample chamber was constructed along the same design with the exception that the sample shield was lengthened to 5-3/8 in. and small hooks were placed inside the shield 1-3/4 in. from the bottom. For the longer samples the loading procedure was the same as described above. However, for the shorter samples the nylon threads were passed over the pulleys and down through the hooks on the inside of the sample shield and then connected to the sample. This allowed the sample to be supported at a point 3-1/2 cm from the bottom of the sample chamber.

A slit was cut in the sample shield near the top of the sample for the sample thermal ground. Once the short sample was mounted a long quartz spacer was installed and the remainder of the assembly was carried out as described above.

Dewar System

For an experiment of the present sensitivity dewar design becomes quite important for the elimination of magnetic, eddy current, and vibrational effects. The introduction of a glass dewar system eliminated the magnetic and eddy current problems and a simple innertube suspension system has eliminated a greater part of the vibrations (see Figure 3).

The present glass dewar system was designed with a large bulge to contain sufficient liquid helium for a ten or twelve hour run. The long tail of the helium dewar was designed so that very long samples (up to 20 cm) could be used if desired to increase sensitivity. In this case there still would be sufficient liquid helium above the sensor coil for a five or six hour run. It was also decided to seal the nitrogen dewar so that the liquid nitrogen could be pumped down to its freezing point. The bubbles from liquid nitrogen at one atmosphere cause vibrations of about 5Å. If the nitrogen is pumped down to its freezing point and sealed-off, no boiling will occur until its vapor pressure has again reached one atmosphere. It generally takes five hours after pump-down is completed to boil again.

The dewar system and liquid coolants combined weigh about 200 pounds. This system is suspended rigidly from a 1/2 in. thick aluminum plate which is supported on two small innertubes which lie on the support frame. These

Figure 3. Schematic drawing of glass dewars and dewar system support

DEWAR SYSTEM

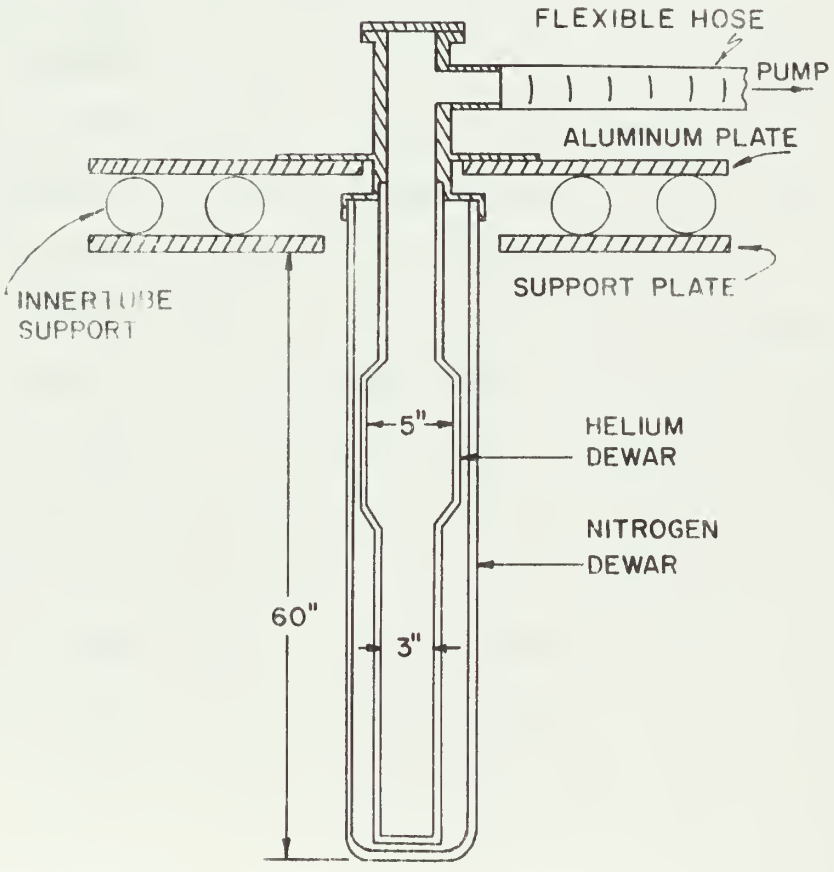

innertubes act as very effective dampers for frequencies of the order of 10 to 20 c/s which form the major vibrations external to this experiment. The pressure in the innertubes is of the order of five psig and may be varied to adjust the damping constant of the system. All pumping and sensing lines have at least a small section of rubber hose in them to maintain the flexibility of the system.

Heater Supply

The temperature of the sample is raised by passing a small current through a 40 Ω heater wire (number 44 manganin) which is wound around the sample and is attached with G.E. 7031 adhesive. The power used is of the order of 20 milliwatts at 30°K. A center tap and each end of the heater wire are connected to a low current power supply in such a manner that current can be passed through either the whole heater or only through one-half. This is done so that thermal gradients across the sample can be detected by comparing "end only" measurements with "total" measurements.

The current supply is a transistorized current source which will provide direct currents from 0 to 400 ma in four ranges to a low resistance load. The lower ranges are used in taking data at liquid helium temperatures while the upper ranges are used for systems checks at room and liquid nitrogen temperatures. A change in line voltage of 20% or a doubling of the load will change the current by on 0.1%. This stability is necessary since small fluctuations in the heater current will produce significant fluctuations in temperature.

Mutual Inductance Circuit

The variable transformer consists of a fixed primary coil, a movable secondary coil, and an additional pickup coil wound around the primary turns (see Figure 4) so that a modified mutual inductance bridge can be used. The primary coil is wound in three sections where the ends (1/4 of the coil length each) are wound in one direction and the center half is wound in the other. This provides a field configuration as shown in Figure 5. The important features of this configuration are that the field approaches zero rapidly at the ends of the coil thereby reducing eddy currents in the sample and sample chamber which may produce heating or erroneous signals in the mutual inductance bridge. The middle and end "humps" are flat to about 0.1% over about 1mm. The pickup coil is wound directly over the primary coil in the same manner to provide maximum linkage.

The secondary coil is made in two halves wound in opposite directions. The length of the secondary coil is such that when the coil is centered the ends of the secondary coil lie on the end "humps" of the primary field. Therefore, when the secondary is situated midway with respect to the primary field there is no net flux linkage. As the secondary coil is moved with respect to the primary coil a small distance a voltage is induced in the secondary coil whose phase differs by 180° depending upon the direction of movement. The magnitude of this voltage is proportional to the coil off-set. Since the sample is attached mechanically to the secondary coil, the voltage produced will be a direct measurement of the sample expansion.

The axial magnetic field at the center of the primary coil divided by the primary current can be expressed by

Figure 4. Linear variable transformer and winding data

VARIABLE TRANSFORMER

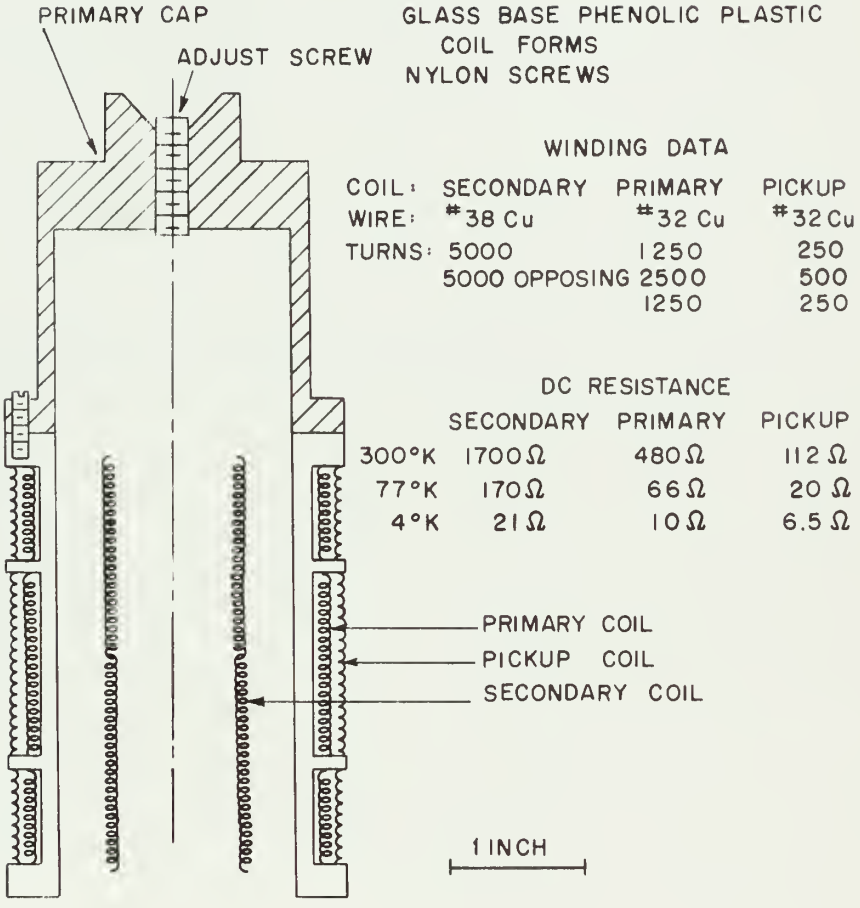

Figure 5. Primary field configuration with magnitude corresponding to a primary current of 100 ma

PRIMARY INDUCTION FIELD

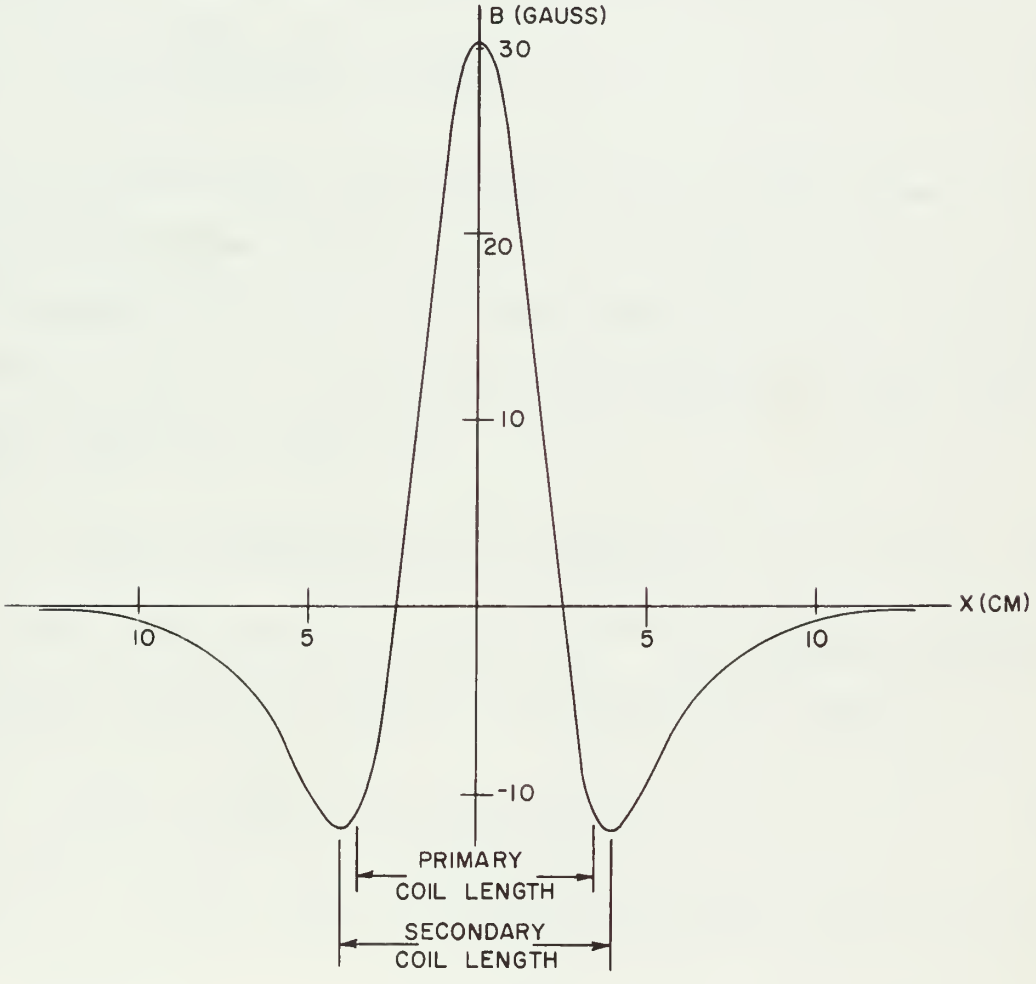

$$B_o/I_p = \mu_o n_p \gamma \quad , \tag{36}$$

where μ_o is the permeability of free space, n_p is the number of turns per unit length of the primary coil, and γ is a geometrical factor (about 0.7 for the present coil). B_o for the present coil is about 300 gauss/ampere. The mutual inductance between the secondary and primary coils is

$$M = \frac{A_s n_s}{I_p} (2z'B_o - 2z'B_1) \quad , \tag{37}$$

where A_s is the mean area of the secondary coil, n_s is the number of turns per unit length of the secondary coil, B_1 is the magnetic field at the end of the secondary coil (i.e. at the "hump"), and z' is a small displacement from the null position. However, $B_o - B_1$ can be expressed as ΓB_o, where Γ is another geometrical factor, so

$$M(z') = (2/I_p)(A_s n_s B_o \Gamma z') \cong 2A_s n_s n_p \mu_o z' \quad , \tag{38}$$

since $\gamma\Gamma \cong 1$. This coupling is about 8×10^{-10} henries/$\mathring{A}$ for the present transformer. The induced voltage in the secondary coil then is

$$E(z') = -M \frac{dI_p}{dt} = -2\omega A_s n_s n_p \mu_o I_p z' \quad , \tag{39}$$

where ω is the angular frequency of the primary current. Thus the sensitivity is given by

$$\frac{d\,E(z')}{d\,z'} = 2\omega A_s n_s n_p \mu_o I_p \quad . \tag{40}$$

For the present experiment where $\omega/2\pi$ is 250 c/s, I_p is 100 ma, and A_s, n_s and n_p are given in Figure 4,

$$\frac{\Delta E(z')}{\Delta z'} \simeq 0.3 \text{ m}\mu\text{v}/0.01\text{Å} \quad . \tag{41}$$

It was apparent in the earlier work (5) that the stability and range of the various "standard" mutual inductances of the conventional Hartshorn bridge caused serious limitations to both the sensitivity and the precision of the measurements. For these reasons a ratio transformer was incorporated into a modified mutual inductance bridge (see Figure 6). In this way the mutual inductance between the primary and secondary coils is cancelled by the fraction of the mutual inductance between the primary and pickup coils which is determined by the ratio transformer setting. The pickup coil and the ratio transformer therefore replace the variable inductance of the Hartshorn bridge and allow a relative range of 10^{10} which is accurate to 0.001% of the full scale reading, which does not drift with temperature, and which can not be changed by vibration or jolting.

For ease of calibration, it is convenient to have an effective bridge length of more than one millimeter. At the same time the least count of the experiment is 0.01Å so a range of at least 10^9 is necessary. It was decided to design for a range of 10^{10} with a full scale value of one centimeter to insure that at least the one millimeter range was achieved. The ratio transformer used in the present experiment is a modification of two Gertsch model 1011R seven decade ratio transformers connected to provide a range of 10^{10} (see Figure 6). The inputs of these two transformers from the pickup coil are connected in parallel. The high side of one of the transformers is the high side of the ratio transformer complex. The output of the other transformer is reduced by 1000:1 transformer handwound around

Figure 6. Mutual inductance bridge circuit

MUTUAL INDUCTANCE BRIDGE

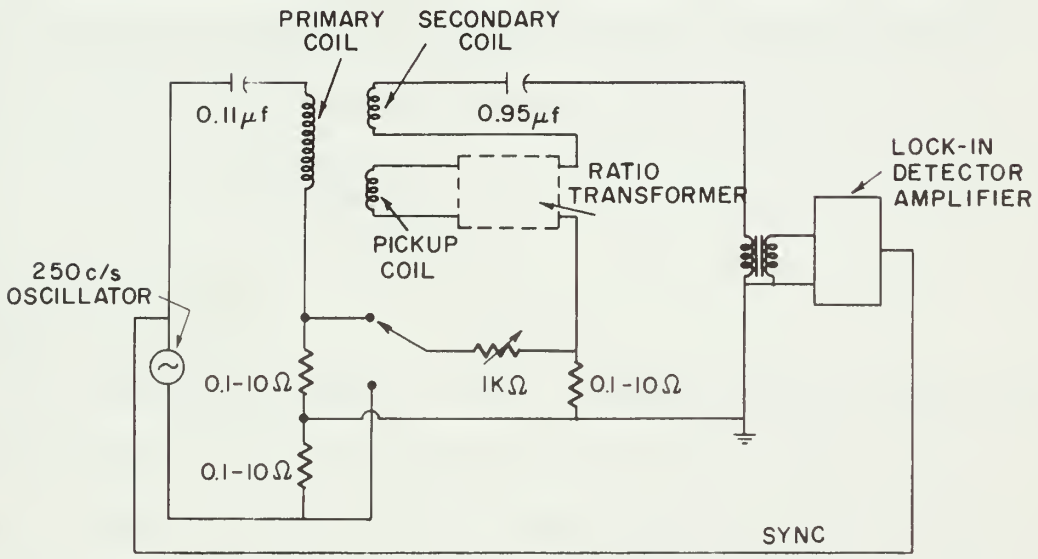

RATIO TRANSFORMER

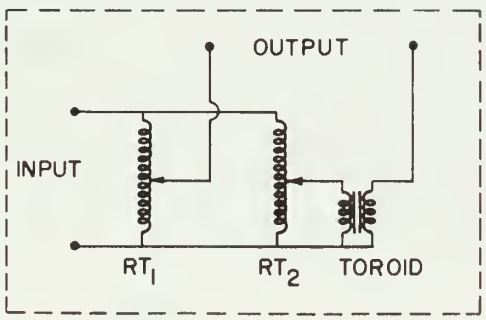

a Supermalloy toroid core. The high side of the output of the toroid transformer is the low side of the ratio transformer complex. In this way the second ratio transformer has a range of 10^7 which starts at 10^{-3} of the first ratio transformer, so a total range of 10^{10} is achieved. Since the mutual inductance between the primary and the pickup coils should equal the mutual inductance between the primary and the secondary coils when z' is 1cm, the number of turns on the pickup coil is

$$N_{pu} \simeq \frac{2A_s n_s z'}{A_{pu}} \quad , \tag{42}$$

or about 1000 turns.

The alternating voltage source is a variable frequency power oscillator, Optimation model AC-15. The primary loop is series-tuned so that a lower output voltage can be used from the oscillator for a given primary current. The gain and the frequency of the oscillator are stable to within 0.01% over a twenty-four hour period. This is necessary since a fluctuation in either of these settings will affect the balance point significantly due to capacitive pickup between the various coils and to other non-idealized elements in the circuit. Two dropping resistors (0.1 to 10 ohm) are included in the circuit to cancel resistive components. The amount of voltage across these resistors is regulated by a 1KΩ rheostat which controls the current in the resistive loop.

The null voltage in the secondary loop is detected by a narrow-band, low noise, lock-in amplifier-detector (29). The amplifier has a low noise input ($\pm$ 0.05 vrms with a one second time constant) and a low microphonic response. The least count signal to the amplifier is increased by a factor

of 500 through the use of an S.I.E. model D15549 input transformer. The null is observed on a d.c. ammeter output from the lock-in detector. An oscilloscope is used to monitor the phase of the signal.

In working with a mutual inductance system where changes of a few parts in 10^{11} of the flux linkage are important, many problems are encountered which would not be significant in a system of lower sensitivity. In this experiment, considerable time was spent in isolating and eliminating second and third order effects. It is worthwhile to discuss some of these problems and their solutions even through in many cases it is not known which of several possible causes led to spurious effects. These problems will be discussed in two categories: magnetic and eddy current effects and grounding effects.

In an ideal bridge, a change in the primary current should not cause a change in the balance. However, if a magnetic material is present in the vicinity of the sensor coil this is not the case since the permeability $\mu = \mu(H)$. For example, in the first stages of this experiment a 1% change in primary current caused a shift in the balance point of 10^{-5} on the ratio transformer (full scale being unity). Subsequently it was found that nichrome wire had mistakenly been used instead of a non-magnetic wire to suspend the sample chamber from the top of the dewar and that these wires ran along the outside of the sensor coil. When these wires were replaced with linen thread the current effect was reduced by a factor of 500. This current effect was reduced even further by replacing the Kovar seal on the glass envelope by a copper-to-glass "housekeeper" seal. Since the oscillator now in use has an amptitude stability of 0.01% the current effect (which appeared as drifts or noise) is no longer a factor in the

measurements.

A more subtle problem was encountered when the required sensitivity and noise level were obtained. A 10 cm long sapphire sample was installed and an experimental run was attempted to compare the results with data taken two years ago on an interim apparatus. The results obtained indicated that there was a large anomalous "expansion" as shown in Figure 7. The two most significant points of interest in these results are the regions of apparent negative expansion at about 11.5°K and 26°K. The lower region was found to be primary field dependent, but not a function of bath temperature. The upper region, on the other hand, was found to be independent of primary field, a function of bath temperature, and larger than the lower effect by a factor of 3.

Au-Fe thermocouples had been installed to monitor the temperatures of the secondary coil and the sample thermal ground. Part of the anomalous behavior may have been a result of the localized magnetic moments in the thermocouples so these were removed. Also, stainless steel screws which were used to adjust the tension on the nylon sample support threads were replaced with brass and the sample thermal ground was simplified. When these changes were completed another run was made and the upper dip had disappeared, the lower dip was slightly reduced, and with the exception of the lower region the data from this run and that of the previous experiment were identical.

No further adjustments were successful in eliminating the lower dip so a new sample holder was constructed. Another run was made with results which were within 1% of those obtained two years earlier. It is believed that this success was due to the use of Cd-Bi non-superconducting solder for

Figure 7. Anomalous results due to various magnetic and eddy current effects in the thermal expansion apparatus

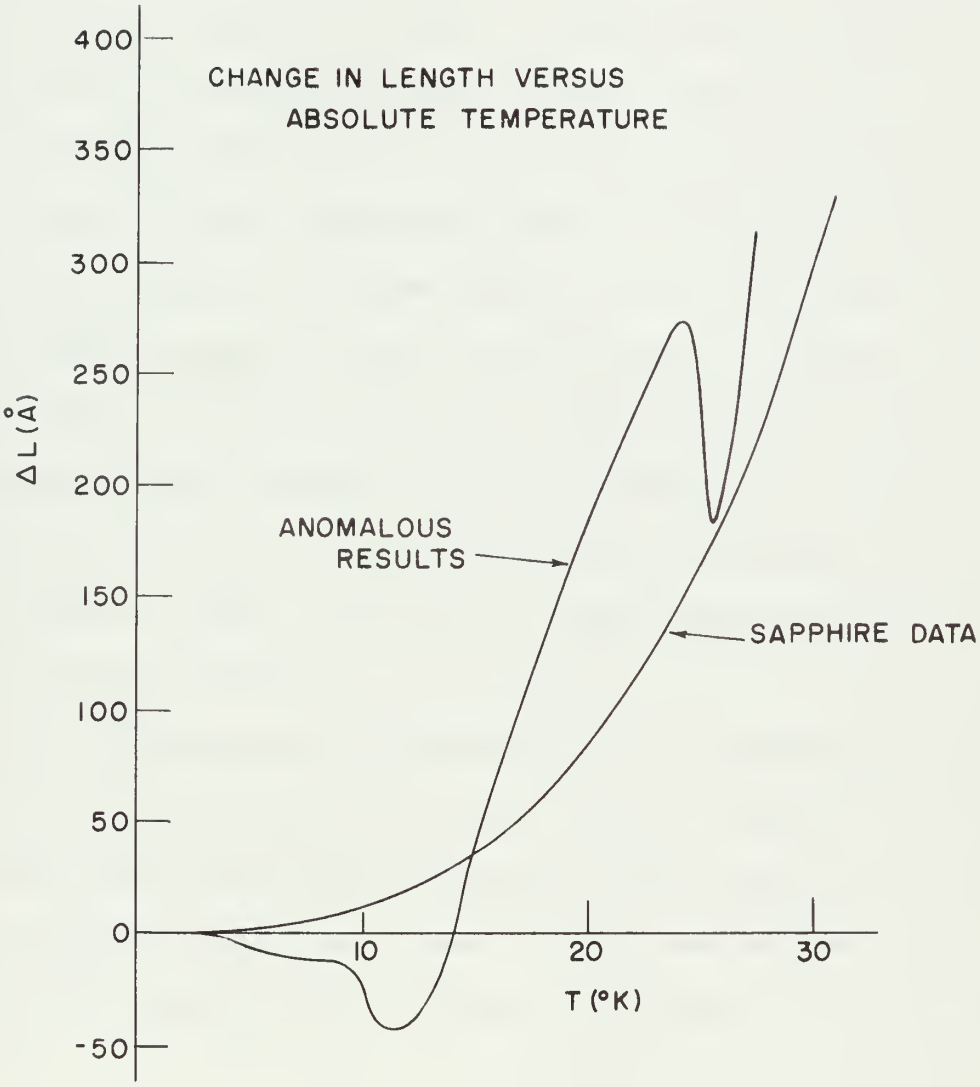
CHANGE IN LENGTH VERSUS
ABSOLUTE TEMPERATURE
400
350
300
250
200
150
100
50
0
-50
ΔL (Å)
ANOMALOUS
RESULTS
SAPPHIRE DATA
10
20
30
T (°K)

all connections in the vicinity of the sensor coil and to the use of high purity copper (99.999%) in all places where copper was used in the sample chamber. This can be important as it has been found that small amounts of magnetic impurities in copper can result in a rapidly varying susceptibility as a function of temperature (30). It is not certain if these two possibilities were the cause of the lower dip, but they seem to be most probable.

In a mutual inductance circuit such as the one described here one must be very careful with the grounding system. In principle it should be possible to establish the system ground at any point in the circuit as long as the rest of the system is isolated properly. However, due to the juxtaposition of large grounded metal objects such as the dewar frame and the electronic rack and their capacitive coupling with the elements of the circuit, it was found that the system ground must be placed at the low side of the detector input. If this was not done large spurious signals resulted in the circuit.

It is also necessary to eliminate all high empedance paths between any high potential element and ground or another element. It was found, for example, that the five-way connectors on the inputs and outputs of the ratio transformers had a capacitance of 300μf between them. These were removed and replaced by BNC connectors. All lead wires were thoroughly shielded. It also is necessary to eliminate even minor ground loops. These wiring faults would cause anything from complete signal saturation to changing the ratios on the ratio transformers.

Thermometry

This experiment was designed to operate in the temperature range between $2^{\circ}K$ and $30^{\circ}K$. In order to obtain an accuracy comparable to that of the calibration of the mutual inductance bridge (0.2%) it is necessary to have an absolute temperature determination of $\pm 0.01^{\circ}K$. In this experiment this criterion is met by the use of an Au-Fe (0.07 atomic percent) versus Cu differential thermocouple referred to the bath temperature (27). This thermocouple has a sensitivity of about $14\mu v/^{\circ}K$ throughout the operating temperature range so voltages of up to $450\mu v$ must be measured to $\pm 0.1\mu v$. These voltages are on the lower ranges of commercial potentiometers, and because of the small absolute voltages involved, it was decided to construct a direct current nulling circuit (see Figure 8).

One junction of the thermocouple is glued to the sample and the other junction is in the helium II bath. The two copper leads of the thermocouple lead to room temperature and the thermocouple voltages would normally be detected between them. However, the nulling circuit is constructed by placing a small resistor, r_d ($0.6443 \pm 0.0003\Omega$), in series with one of the two copper leads that are then connected to a Kiethley model 150 microvoltmeter. An independent pair of leads is used to pass a small current through this resistor to produce sufficient voltage to "buck-out" the thermoelectric voltage. The null is detected on the microvoltmeter. A standard resistance, $R_s = 1000\Omega$, is placed in series with the current source and the voltage drop across this resistor, V_s (as measured by a Keithley model 662 differential voltmeter), is proportional to the thermocouple voltage, V_T, and is given by

Figure 8. Thermocouple measuring circuit

THERMOCOUPLE CIRCUIT

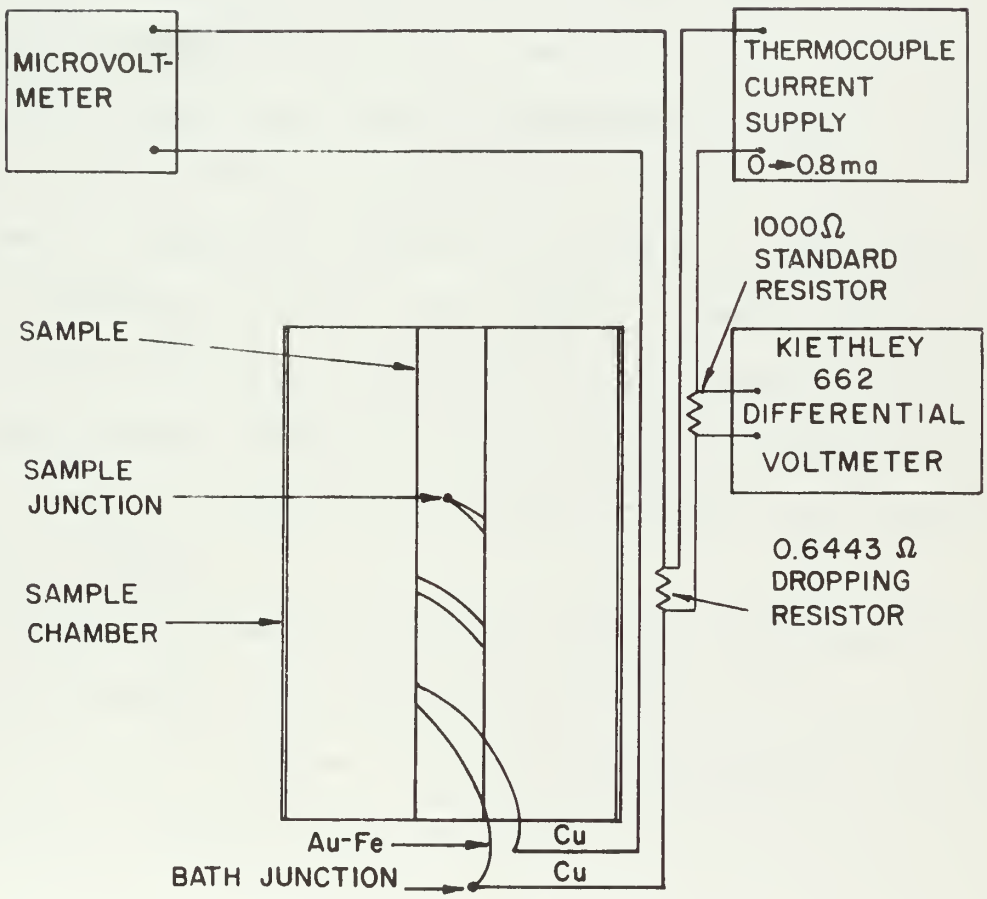

$$V_T = \frac{r_d}{R_s} V_s \quad . \tag{43}$$

The ratio r_d/R_s is determined at 1.9°K by replacing the null detector with a microvolt potentiometer, and then comparing the zero ΔT voltage drops across the thermocouple leads (or r_d) and R_s for a fixed current through r_d and R_s.

It is seen that V_s will be a maximum of about 0.7 volts (when the sample temperature is 30°K) and must be determined to $\pm 155\mu v$ for ± 0.01°K. Since all other connections in the circuit with the exception of the sample junction and the connection at the null indicator are in liquid helium II only small (less than 1.0 μv) constant thermoelectric voltages are developed. The thermoelectric voltage at the connection at the null indicator is kept small since this connection is thermally anchored to a copper plate and encased in styrofoam. The total stray voltages indicated at the microvoltmeter are of the order of $1\mu v$, and do not vary more than $\pm 0.1\mu v$ over ten hours. These voltages are measured when the system is in thermal equilibrium with the bath (no sample heat) and used to correct the differential thermocouple voltages.

The current source must be stable to 0.01% over short periods of time (during a measurement). Since the maximum current is only 0.7 ma, a bank of nine mercury cells connected in series is quite successful in providing the voltage for a standard d.c. current supply.

CALIBRATION

Since the total linear bridge length was designed to be well in excess of one millimeter and calculations indicated that the primary field should be linear to better than 0.5% over this range a direct calibration was used. This method involves using a traveling microscope slide to move the secondary coil with respect to the primary coil (see Figure 9). This instrument can be read with care to ± 1 micron. The sensing coils are placed in liquid nitrogen to take into consideration the thermal contraction of the coils between 300 and 77°K, and to increase the sensitivity of the bridge by reducing the resistance of the coils. One calibration run was performed at liquid helium temperatures as a check and the same results were obtained.

For the "top half" of the coil, the calibration of the sensing coils is $\Delta L = 1.130(\pm 0.001)\ \Delta n$ cm where $n < 1$ is the ratio transformer reading, i.e. 1.130 cm for the full bridge range, $\Delta n = 1$ (see Figure 10). The "top half" of the coil is defined such that the center of the secondary coil is above the center of the primary coil. The calibration of the "bottom half" is a few percent less than the "top half", but since it is not as linear (about 0.4%) the "bottom half" is not normally used to take data.

It should be emphasized that the use of this calibration depends upon the fact that the variable transformer remains linear (or becomes more linear) as the range of motion decreases. Therefore, the calibration obtained over a larger range can be trusted when making small measurements. This can be checked somewhat by running a sample at different bridge settings and checking the results. This was done and no discrepancies were found.

Figure 9. The calibration apparatus

COIL CALIBRATION APPARATUS

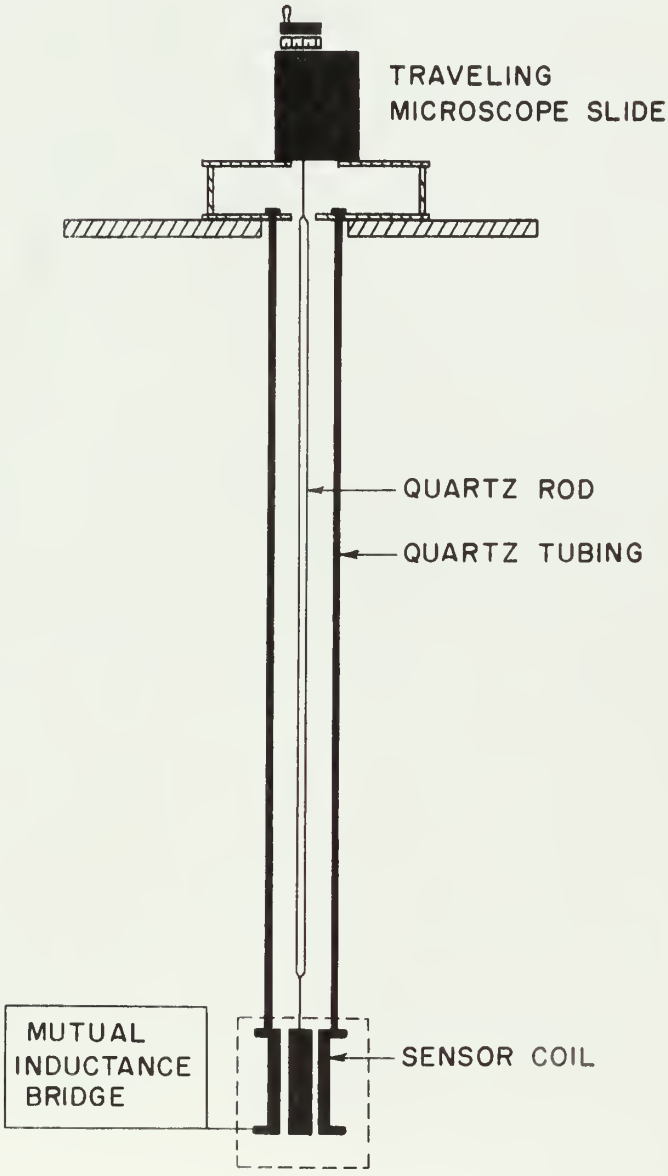

Figure 10. Linear variable transformer calibration where Δn is the difference in ratio transformer settings

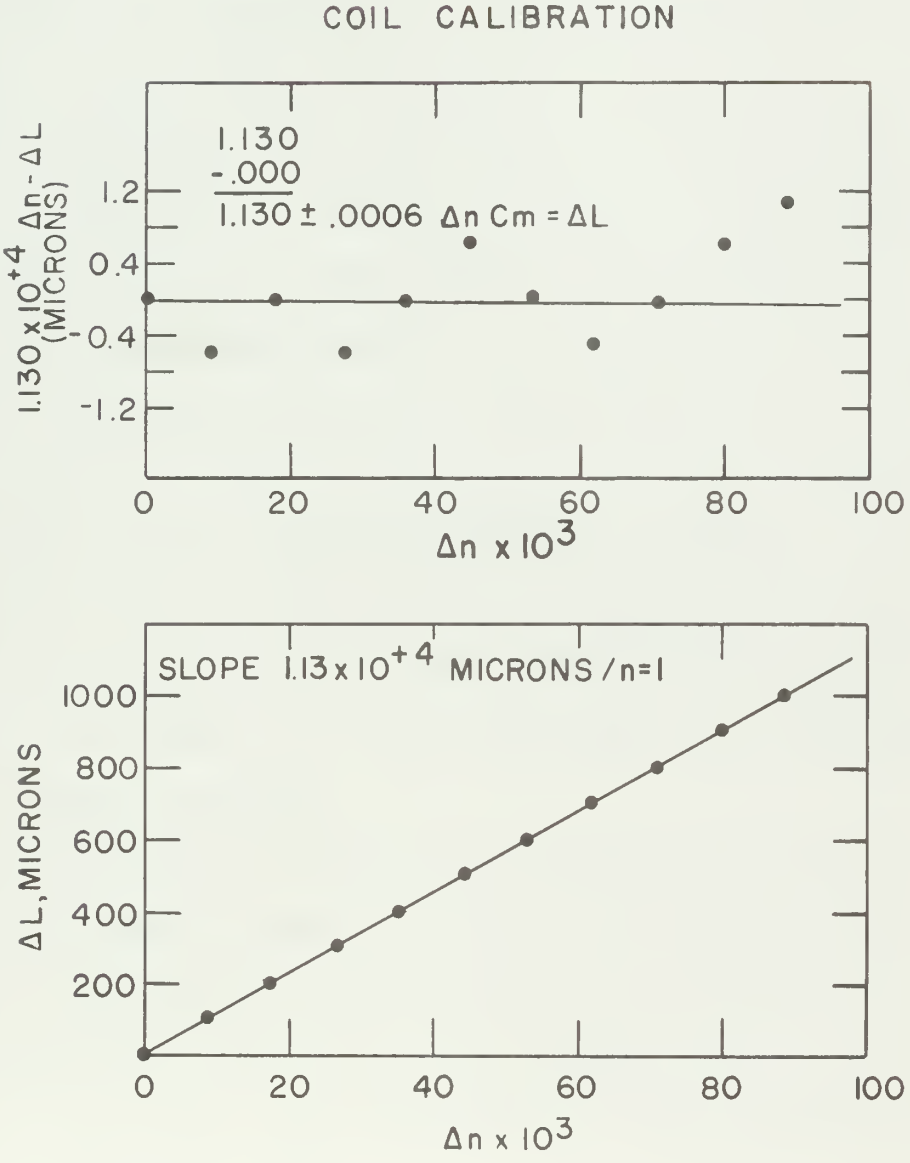
COIL CALIBRATION
1.130
-.000
1.130 ± .0006 Δn Cm = ΔL
1.130 x 10+4 Δn - ΔL (MICRONS)
1.2
0.4
-0.4
-1.2
0
20
40
60
80
100
Δn x 10^3
SLOPE 1.13 x 10+4 MICRONS / n=1
ΔL, MICRONS
1000
800
600
400
200
0
20
40
60
80
100
Δn x 10^3

EXPERIMENTAL PROCEDURE

The various components of the system have been described above. The inter-relationship of these can be appreciated better through a description of the procedure involved in the performance of an experiment. Three steps are involved; sample preparation and loading, systems check and helium transfer, and the method of taking data.

The samples used in this experiment vary in length from 7 cm to 13.5 cm and are about 1/4 in. to 3/8 in. in diameter. As described above the 10 cm samples are used in sample chamber I while the shorter and longer samples are used in sample chamber II. In preparation, the sample ends are polished normal to the sample axis and the sapphire disks are glued to the ends with G.E. 7031 adhesive. The heater wire is wound astatically on the sample and glued, and then the thermocouple is attached in the same way making sure that good thermal contact is maintained along two or three inches of the sample. All electrical connections are made, the sample is mounted on the sapphire ball, the quartz spacer rod is installed, and the sample chamber is assembled.

After the primary coil has been installed and the pumping line attached, the sample chamber is pumped and flushed with nitrogen gas several times and then leak-detected. A rough balance is set with the primary coil and the whole apparatus then is placed in the dewar where it rests on the bottom. This is done so the measurements will not be affected by small changes in the dewar length.

Once the apparatus has come to equilibrium at $77^{\circ}K$ and before liquid helium is transferred the heater, mutual inductance, and thermometry

circuits are checked out once again. It usually is not necessary to rebalance the primary since there is sufficient range on the rough balance at room temperature to compensate for any differential expansion (which could be ~0.3mm). Once these prechecks are completed the helium dewar, vacuum chamber, and the sample chamber are sealed-off. Liquid helium then is transferred and after another set of systems checks are made, the bath is pumped down to 1.89°K and regulated by a cartesian manostat. After about one hour the whole system has settled down and data can be taken.

In this experiment there are two distinct types of data taken; at the lowest temperatures a continuous record of ΔL versus temperature was taken every few tenths of a degree. At higher temperatures five points are taken over a small temperature range (about 0.3°K) and fitted with a straight line to obtain the thermal expansion coefficient, α, directly, where $\alpha = \frac{1}{L_o} \left(\frac{\partial L}{\partial T}\right)_p$ (see Figure 11). The α points were taken every one or two degrees and ΔL, a length change, was taken between these points to give a continuous ΔL versus T plot if needed. This could be obtained by integrating the α vs. T data also. Although these two types of data give different quantities the method of taking them is quite similar.

First a base point is established by having the system come to equilibrium with a given heater current (at the lowest temperatures this would be $I_H = 0$). At this point the thermocouple voltage and the mutual inductance are recorded. A small current in excess of the base point current is then put into the heater, the temperature rises, and another point is recorded. It was found to be convenient to use the Kiethley 150 voltmeter readings for the small thermocouple difference readings as data are taken between base points, so as the heater current is increased from a base point the

Figure 11. Typical plot to determine the linear thermal expansion coefficient

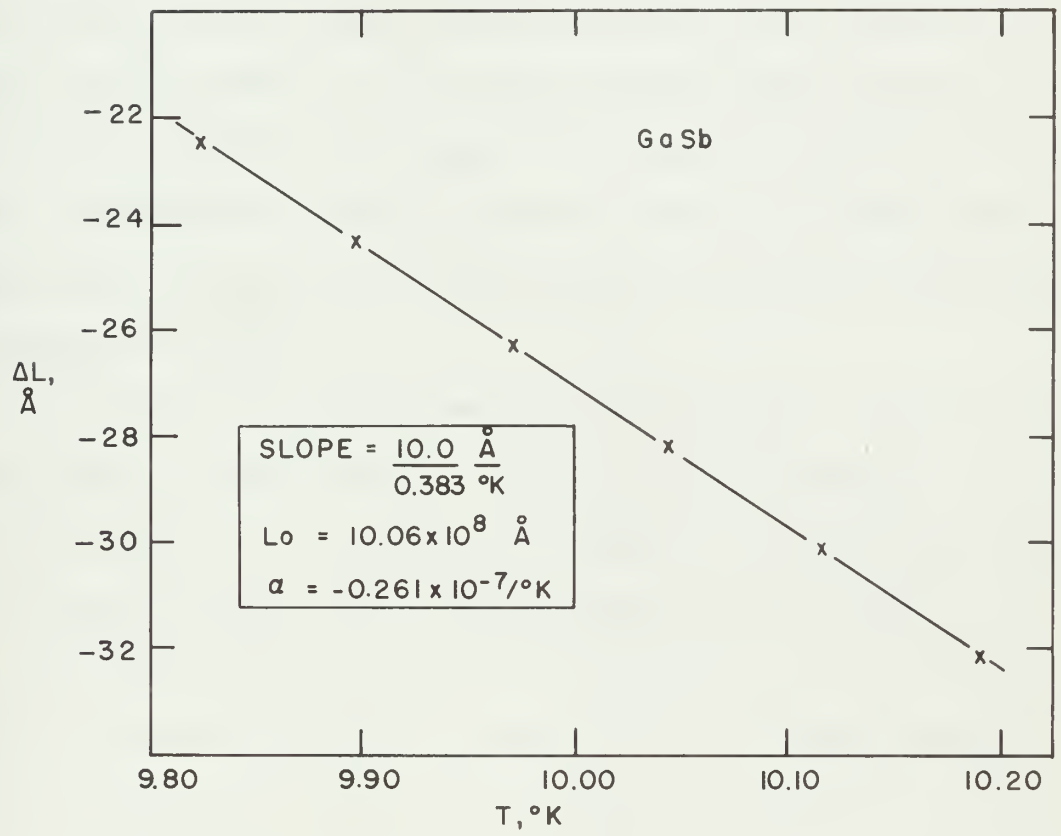
GaSb
SLOPE = 10.0 Å / 0.383 °K
Lo = 10.06 x 10^8 Å
α = -0.261 x 10^-7/°K
ΔL, Å
-22
-24
-26
-28
-30
-32
9.80
9.90
10.00
10.10
10.20
T, °K

thermocouple voltage difference is read on the Kiethley up to 10 $\pm$ 0.1 μv (about 0.7°K). The linearity of the meter readings of the microvoltmeter used in this experiment was checked and found to be 1%. When the thermocouple reaches 10 μv a new base point is established and the process continued. Normally a reading is taken every 2 μv so that about seven points per degree are taken. To get the total length change the base point lengths then are added. In this experiment this method was continued until the thermal expansion of the sample became negative and then α points were taken. The method for obtaining α was the same as at lower temperature except that five points were taken above the base point at thermocouple voltage intervals of 1 μv.

In taking all of these points at least two sets of data were taken at every base point (up to twelve sets at the lowest temperatures) and the data averaged. This allowed for a mean scatter of $\pm$ 0.02$\mathring{A}$ where needed even though the least count of the apparatus was only $\pm$ 0.05$\mathring{A}$. Also some data were taken with only one half of the heater in use to check the temperature distribution across the sample. Points also were taken both up and down in temperature to insure that there was no hysteresis in the expansion. In all cases the base point was returned to repeatedly insuring that there were no drifts or jumps in the balance point while data were being taken.

RESULTS

In this experiment thermal expansion measurements were performed on Si, Ge, GaAs, GaSb, InAs, and InSb. These materials were chosen since they form a group centered around Ge on the periodic chart and it was hoped that correlations would be found which would assist in understanding the behavior of these tetrahedrally bonded solids. The sample properties and sources are given in Table 1. The original 20.5 cm long Ge sample was cut into two pieces, one approximately twice the length of the other, so that data from samples of different lengths could be used to check the apparatus for systematic errors. The samples were prepared and data were taken as described previously. The actual experimental data are presented in the appendix.

Table 1. Sample properties and sources

Sample	$4^{\circ}K$ Length (cm)	Diameter (cm)	Resistivity (Ω-cm($300^{\circ}K$))	Net Carrier* Concentration (atoms/cm^3)	Source
Si	13.65	~0.9	150	$\sim 10^{15}$	Texas Inst.
Ge	13.46	~1.2	48	$<10^{17}$	Mono Silicon
	6.99	~1.2	48	$<10^{17}$	Mono Silicon
GaAs	8.26	~0.6	0.002	$\sim 2 \times 10^{18}$	Texas Inst.
GaSb	10.06	~0.6	0.68	$\sim 10^{17}$	Texas Inst.
InAs	10.01	~0.6	0.012	$\sim 2 \times 10^{16}$	Texas Inst.
InSb	10.12	~1.0	0.024	$<1.6 \times 10^{16}$	Ohio Semiconductors

*The various uncompensated impurity concentrations were determined by comparing the observed resistivities with those of doped samples. Data for Ge, Si, GaSb, and InSb were obtained from Hannay (31), while the information for GaAs and InAs were obtained from unpublished literature supplied by Texas Instruments, Inc. In addition, the reflectivities of Ge and Si were kindly measured by Professor D. W. Lynch, of this laboratory (private communication 1966). These results indicated only that impurity carrier concentrations were less than 5×10^{17}. Helicons were detected in a piece of the InSb sample by J. L. Stanford, also of this laboratory (private communication 1966) indicating the stated purity.

As was expected from earlier work, as the temperature was increased each sample indicated an initial region of relatively small positive thermal expansion which was followed by a region of relatively large negative expansion (see Figures 12 to 17). In about the first two-thirds of these positive expansion regions the length changes of the samples are proportional to T^4. This would be expected from a simple application of the Debye theory. At higher temperatures the region of negative thermal expansion continued to the highest temperatures reached in this experiment ($30^{\circ}K$ - $35^{\circ}K$), although a minimum thermal expansion coefficient, α_{min}, was observed in all cases except for Si.

The mean scatter in the ΔL's in the low temperature positive thermal expansion region was as low as $\pm 0.02\mathring{A}$ for InAs and InSb and for all samples the T^4 coefficients were determined with an accuracy of from 1.5% for Si to 6% for InSb (see Figures 12 to 17). The smoothed values of α and γ_T which are given in Table 2 are believed to be accurate to about 2% up to $22^{\circ}K$. Above this temperature the Au-Fe thermocouple calibration was obtained by extrapolating data taken at lower temperatures, so the ΔT's in this region could be in error by as much as ten percent. A proper calibration at these higher temperatures is planned. The results obtained for Ge and Si in this experiment compare favorably with those of Carr et al. (19) and a comparison of the data is shown in Figures 12 and 13 and in Table 2. It is seen that the data for Ge agree quite well except at higher temperatures where the thermometry in this experiment is in doubt. The data for Si do not agree as well, but the data of Carr et al. are in some doubt due to sample problems (19). It is difficult to compare the results obtained for GaAs, GaSb, and InSb with the data of Novikova (16, 17, 18), since that author's

Figure 12. Linear thermal expansion of silicon

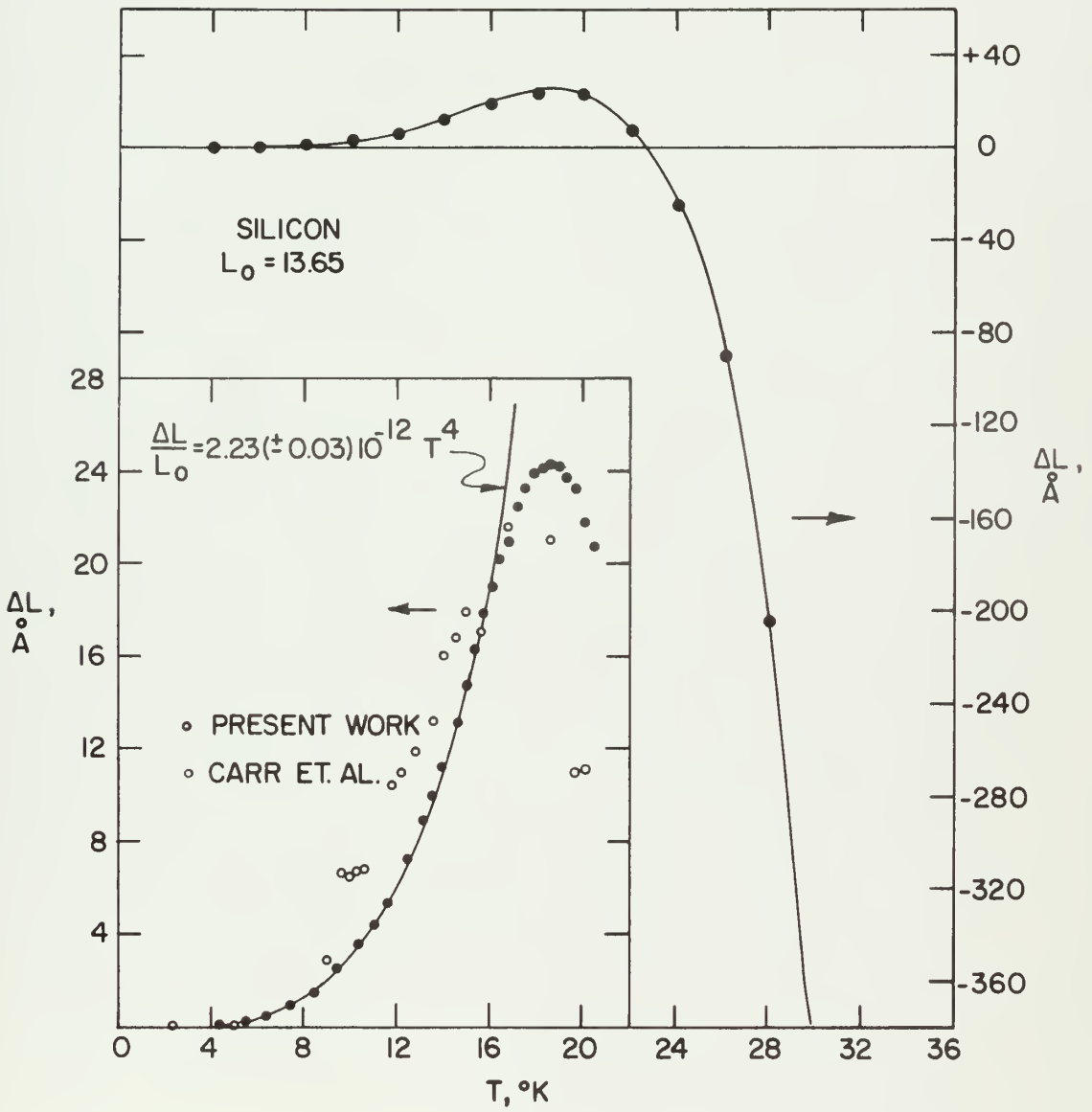
SILICON
L_0 = 13.65
$\frac{\Delta L}{L_0}$ = 2.23(± 0.03) 10^{-12} T^4
PRESENT WORK
CARR ET. AL.
ΔL, Å
ΔL, Å
T, °K
+40
0
-40
-80
-120
-160
-200
-240
-280
-320
-360
28
24
20
16
12
8
4
0
4
8
12
16
20
24
28
32
36

Figure 13. Linear thermal expansion of germanium

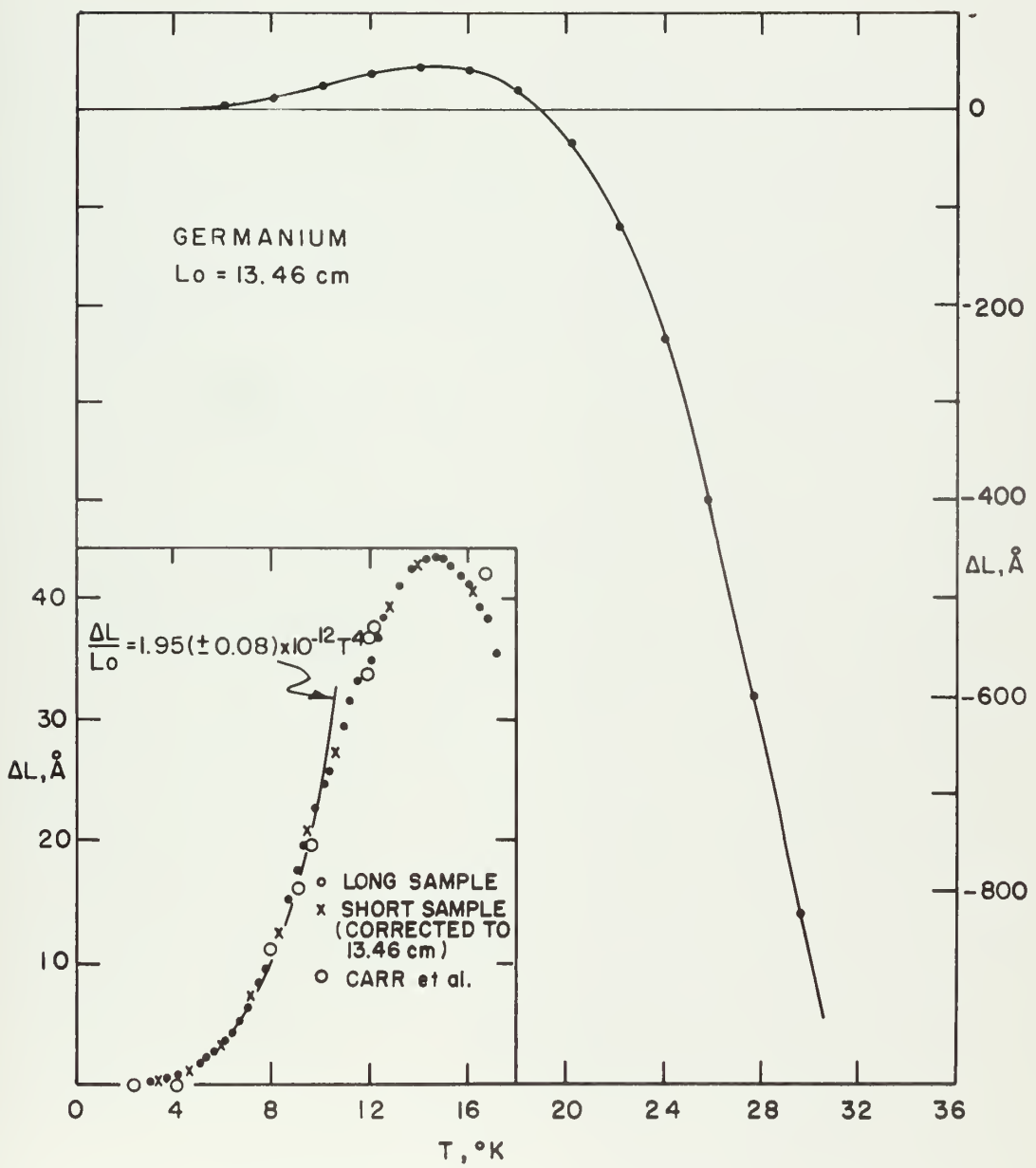
GERMANIUM
Lo = 13.46 cm
0
-200
-400
-600
-800
ΔL, Å
40
30
20
10
ΔL, Å
ΔL/Lo = 1.95(±0.08)x10⁻¹² T⁴
o LONG SAMPLE
x SHORT SAMPLE (CORRECTED TO 13.46 cm)
o CARR et al.
0
4
8
12
16
20
24
28
32
36
T, °K

Figure 14. Linear thermal expansion of GaAs

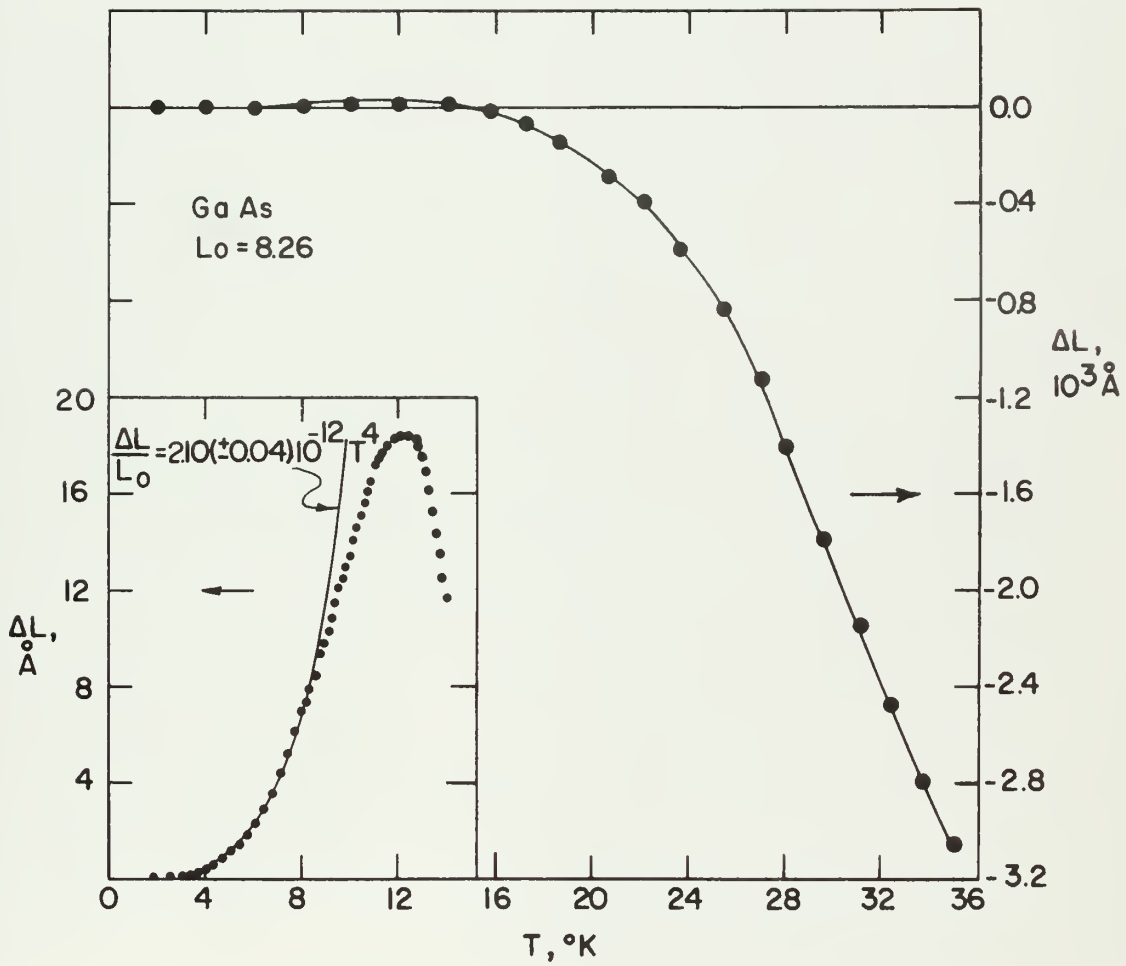
Ga As
Lo = 8.26
ΔL/Lo = 2.10(±0.04)10^-12 T^4
ΔL, Å
ΔL, 10^3 Å
T, °K
0.0
-0.4
-0.8
-1.2
-1.6
-2.0
-2.4
-2.8
-3.2
20
16
12
8
4
0
4
8
12
16
20
24
28
32
36

Figure 15. Linear thermal expansion of GaSb

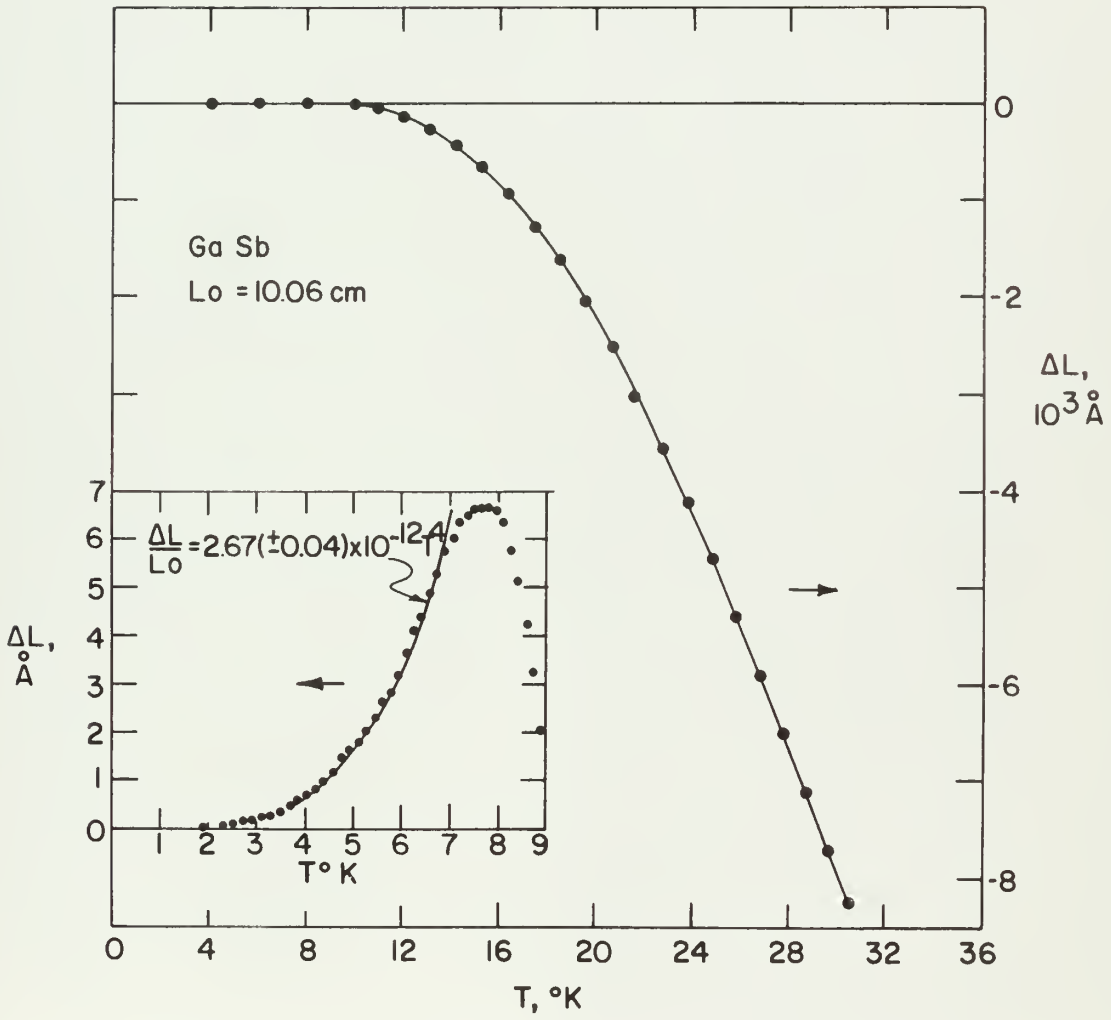
Ga Sb
Lo = 10.06 cm
ΔL, 10³ Å
ΔL, Å
T, °K
T° K
ΔL/Lo = 2.67(±0.04)x10⁻¹²T⁴

Figure 16. Linear thermal expansion of InAs

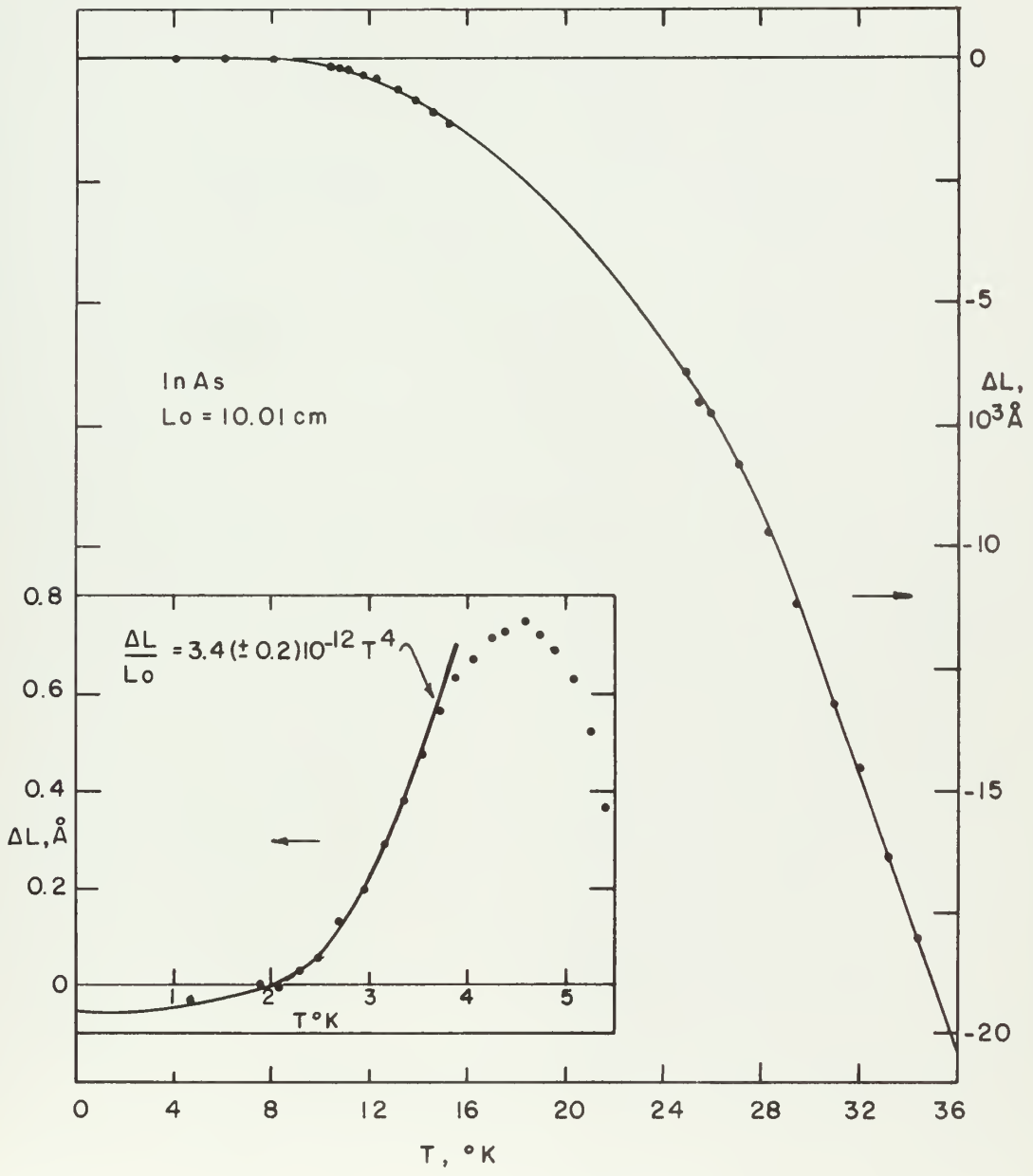
InAs
Lo = 10.01 cm
ΔL, 10³Å
0
-5
-10
-15
-20
0
4
8
12
16
20
24
28
32
36
T, °K
ΔL/Lo = 3.4 (± 0.2) 10⁻¹² T⁴
ΔL, Å
0.8
0.6
0.4
0.2
0
1
2
3
4
5
T°K

Figure 17. Linear thermal expansion of InSb

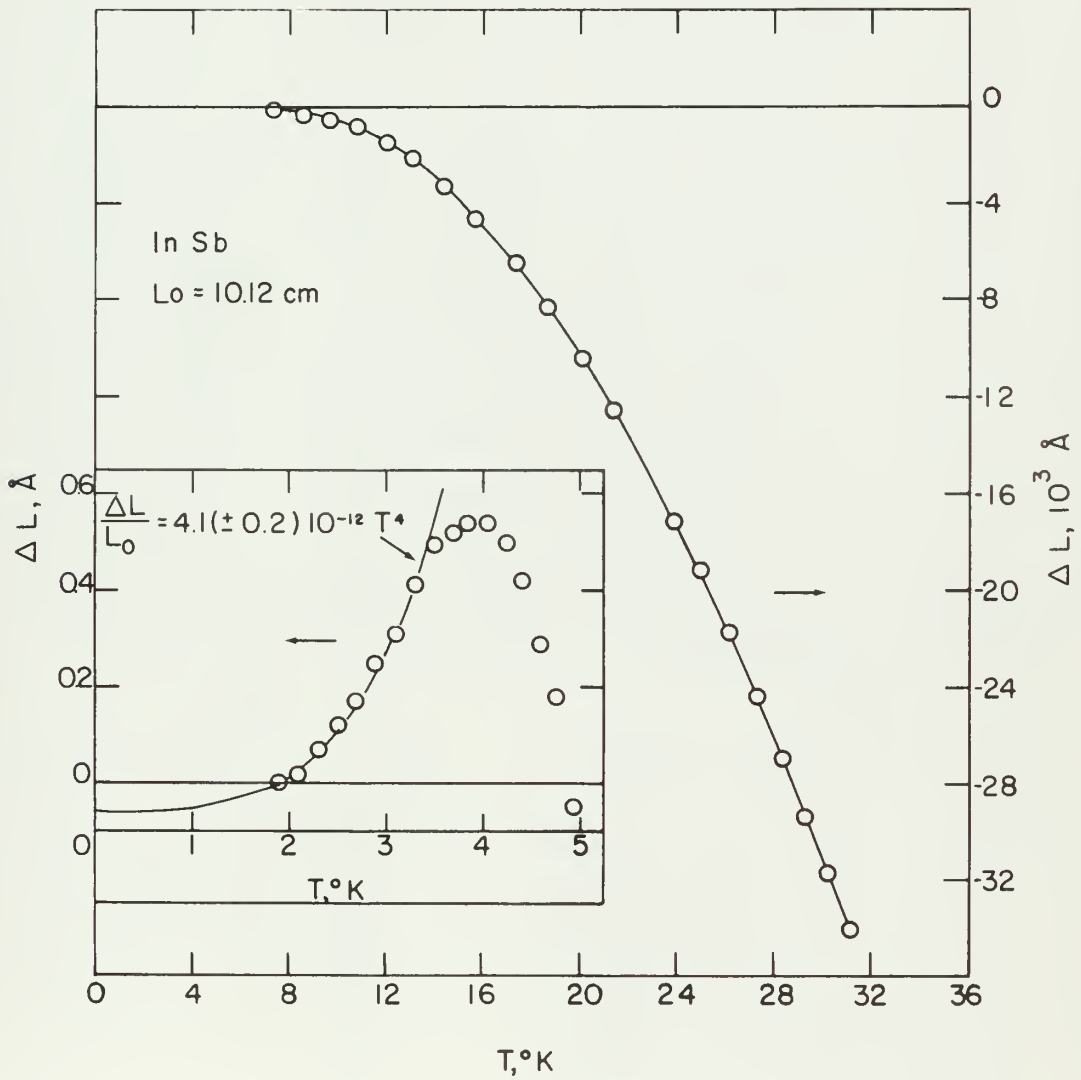
In Sb
Lo = 10.12 cm
ΔL, Å
ΔL, 10³ Å
T,°K
ΔL/Lo = 4.1(± 0.2) 10⁻¹² T⁴
T,°K

Table 2. Smoothed values of α and γ_T

T	Si $\alpha(^\circ K^{-1}) \times 10^8$	Si γ_T	Ge $\alpha(^\circ K)^{-1} \times 10^8$	Ge γ_T
0	0.0	0.44	0.0	0.66
2	7.0×10^{-4}	0.44	6.2×10^{-3}	0.65
4	5.6×10^{-3}	0.44	4.9×10^{-2}	0.63
6	1.9×10^{-2}	0.43	1.7×10^{-1}	0.60
8	4.5×10^{-2}	0.42	0.40 (0.35)	0.53 (0.45)
10	8.8×10^{-2}	0.41	0.50 (0.45)	0.36 (0.25)
12	0.152 (0.15)*	0.38 (0.38)	0.45 (0.60)	0.12 (0.15)
14	0.251 (0.12)	0.34 (0.18)	0.21 (0.25)	0.03 (0.035)
16	0.32 (0.10)	0.26 (0.09)	-0.33 (-0.45)	-0.03 (-0.035)
18	0.18 (-0.08)	0.05 (-0.04)	-1.2 (-1.3)	-0.06 (-0.065)
20	-0.18 (-0.45)	-0.07 (-0.17)	-2.3 (-2.3)	-0.08 (-0.080)
22	-0.70 (-0.85)	-0.15 (-0.21)	-3.7 (-3.6)	-0.10 (-0.092)
24	-1.45 (-1.45)	-0.22 (-0.25)	-5.2 (-4.9)	-0.11 (-0.10)
26	-2.6 (-2.6)	-0.28 (-0.33)	-6.8 (-5.6)	-0.11 (-0.091)
28	-4.3 (-3.8)	-0.33 (-0.36)	-8.2 (-6.1)	-0.11 (-0.084)
30	-6.7 (-5.2)	-0.37 (-0.38)	-9.4 (-7.1)	-0.11 (-0.084)
	$\alpha = 0.88(\pm 0.16) \times 10^{-12} T^3, T < 15.9^\circ K$		$\alpha = 7.80(\pm 0.32) \times 10^{-12} T^3, T < 9.2^\circ K$	

T	GaAs $\alpha(^\circ K^{-1}) \times 10^8$	GaAs γ_T	GaSb $\alpha(^\circ K^{-1}) \times 10^8$	GaSb γ_T
0	0.0	0.56	0.0	0.32
2	6.9×10^{-3}	0.56	8.4×10^{-3}	0.31
4	5.5×10^{-2}	0.54	6.7×10^{-2}	0.28
6	1.9×10^{-1}	0.52	2.26×10^{-1}	0.24
8	4.4×10^{-1}	0.43	-0.18	-0.10
10	0.45	0.25	-2.4	-0.32
12	0.10	0.01	-7.1	-0.43
14	-0.95	-0.11	-12.9	-0.45
16	-2.7	-0.18	-18.8	-0.44
18	-5.1	-0.22	-23	-0.43

Table 2. Continued

	GaAs		GaSb	
T	$\alpha(^{o}K^{-1}) \times 10^{8}$	γ_T	$\alpha(^{o}K^{-1}) \times 10^{3}$	γ_T
20	- 7.7	-0.24	-28	- 0.42
22	-10.5	-0.26	-34	- 0.40
24	-14.0	-0.27	-38	- 0.38
26	-18.0	-0.28	-42	- 0.35
28	-22.6	-0.29	-43	- 0.32
30	-25.6	-0.29	-41	- 0.28
32	-25.4	-0.26		
34	-21.8	-0.21		
	$\alpha = 8.40(\pm 0.16)\times 10^{-12}T^{3}, T<8.0^{o}K$		$\alpha = 10.7(\pm 0.16)\times 10^{-12}T^{3}, T<6.6^{o}K$	

	InAs		InSb	
T	$\alpha(^{o}K^{-1}) \times 10^{8}$	γ_T	$\alpha(^{o}K^{-1}) \times 10^{3}$	γ_T
0	0.0	0.33	0.0	0.19
2	1.1×10^{-2}	0.31	1.28×10^{-2}	0.18
4	0.0	0.00	0.00	0.00
6	-0.25	-0.17	-1.00	-0.46
8	-1.6	-0.39	-9.4	-0.73
10	-5.8	-0.48	-32.1	-0.86
12	-12.5	-0.52	-42.2	-0.88
14	-22.7	-0.55	-63.7	-0.88
16	-33.0	-0.58	-85.3	-0.88
18	-45.2	-0.60	-105	-0.88
20	-58.7	-0.63	-125	-0.87
22	-68.5	-0.65	-144	-0.55
24	-83.0	-0.66	-162	-0.83
26	-97.5	-0.68	-175	-0.81
28	-112	-0.69	-181	-0.77
30	-127	-0.69	-182	-0.72
32	-141	-0.70	-180	-0.66
34	-153	-0.69		
36	-151	-0.68		
	$\alpha = 13.6(\pm 0.7)\times 10^{-12}T^{3}, T<3.5^{o}K$		$\alpha = 16.4(\pm 0.8)\times 10^{-12}T^{3}, T<3.0^{o}K$	

*The values in parenthesis are those of Carr et al. (19).

limits of error are understandably large in the region of overlap (20°K - 35°K) and discrepancies as large as a factor of three occur.

Table 3. Physical constants reduced to 0°K

		Si	Ge	GaAs	GaSb	InAs	InSb
θ_o	°K	645[a]	374[a]	348[b]	267[b]	247[b]	206[b]
C_{11}	10^{11} dynes/cm^3	16.77[c]	13.16[d]	12.26[e]	8.97[f]	8.33[g]	6.66[h]
C_{12}	10^{11} dynes/cm^3	6.50[c]	4.95[d]	5.71[e]	4.12[f]	4.53[g]	3.35[h]
C_{44}	10^{11} dynes/cm^3	8.04[c]	6.84[d]	6.00[e]	4.51[f]	3.96[g]	3.14[h]
B_T	10^{11} dynes/cm^3	9.85[c]	7.65[d]	7.89[e]	5.95[f]	6.02[g]	4.45[h]
a	Å	5.44[i]	5.67[i]	5.66[j]	6.11[j]	6.08[j]	6.50[j]
ρ	g/cm^3	2.33[i]	5.32[i]	5.31[i]	5.62[i]	5.87[i]	5.78[i]
V	cm^3	12.06	13.59	13.55	17.13	16.74	20.45
m	amu	28.08	72.59	72.32	95.73	94.87	118.29
$\Delta C_{11}/\Delta P$		4.29[c]	5.12[k]				
$\Delta C_{12}/\Delta P$		4.20[c]	4.45[k]				
$\Delta C_{11}/\Delta P$		0.75[c]	1.31[k]				

[a] Flubacher et al. (32)
[b] Verma et al. (33)
[c] McSkimmin et al. (34)
[d] McSkimmin (35)
[e] Garland et al. (36)
[f] Einspruch et al. (37)
[g] Gerlich (38)
[h] Potter (39)
[i] Aigrain (40)
[j] Giesecke et al. (41)
[k] Kopperman et al. (42)

The results of thermal expansion experiments are expressed best in terms of the Gruneisen constant, γ, which is defined by equation 23,

$$\gamma = \frac{3\alpha B_T V}{C_V} \quad . \qquad (23)$$

The low temperature value γ_o can be obtained from the limiting region where both the thermal expansion coefficient and the specific heat vary as T^3. The specific heats were calculated using equation 30 and θ_o values obtained from the elastic constants of the various solids. The data necessary to calculate these γ_o's are given in Table 3. In general, γ_o is proportional to $\alpha\theta_o^3/T^3$ and the errors in both α/T^3 and θ_o^3 are believed to be the same order of magnitude.

In order to determine the temperature dependence of the Gruneisen constant (γ_T) it is necessary to know the temperature dependence of the specific heats. Neither of the other parameters (V, B_T) exhibit a significant temperature dependence. Unfortunately, low temperature specific heat data exist only for Ge and Si (32) (where $T/\theta_o \geq 0.01$) and for InSb (43) ($T/\theta_o \geq 0.03$). The specific heats of the other materials (44) have been measured only down to 14°K ($T/\theta_o \geq 0.05$). These data are not adequate for these γ_T calculations. An extrapolation of the existing specific heat data was performed using a reduced plot of the existing data of the form θ/θ_o versus T/θ_o (see Figure 18). The extrapolation of the incomplete data was made by comparison with the reduced plots for Si and Ge using the θ_o values in Table 3. One striking feature (shown in Figure 18) is that at no temperature does θ appear to be constant so the true T^3 region for the specific heat appears only well below $T/\theta_o = 0.01$. It is possible that errors in θ as large as five percent may result from this procedure, but the variation in θ is more than 30% so at least a realistic value of θ (and therefore C_V) may be obtained by this method. The actual values of C_V were

Figure 18. Reduced θ_o versus reduced T curves used for the extrapolation of C_V data to low temperatures with θ_o as given in Table 3.

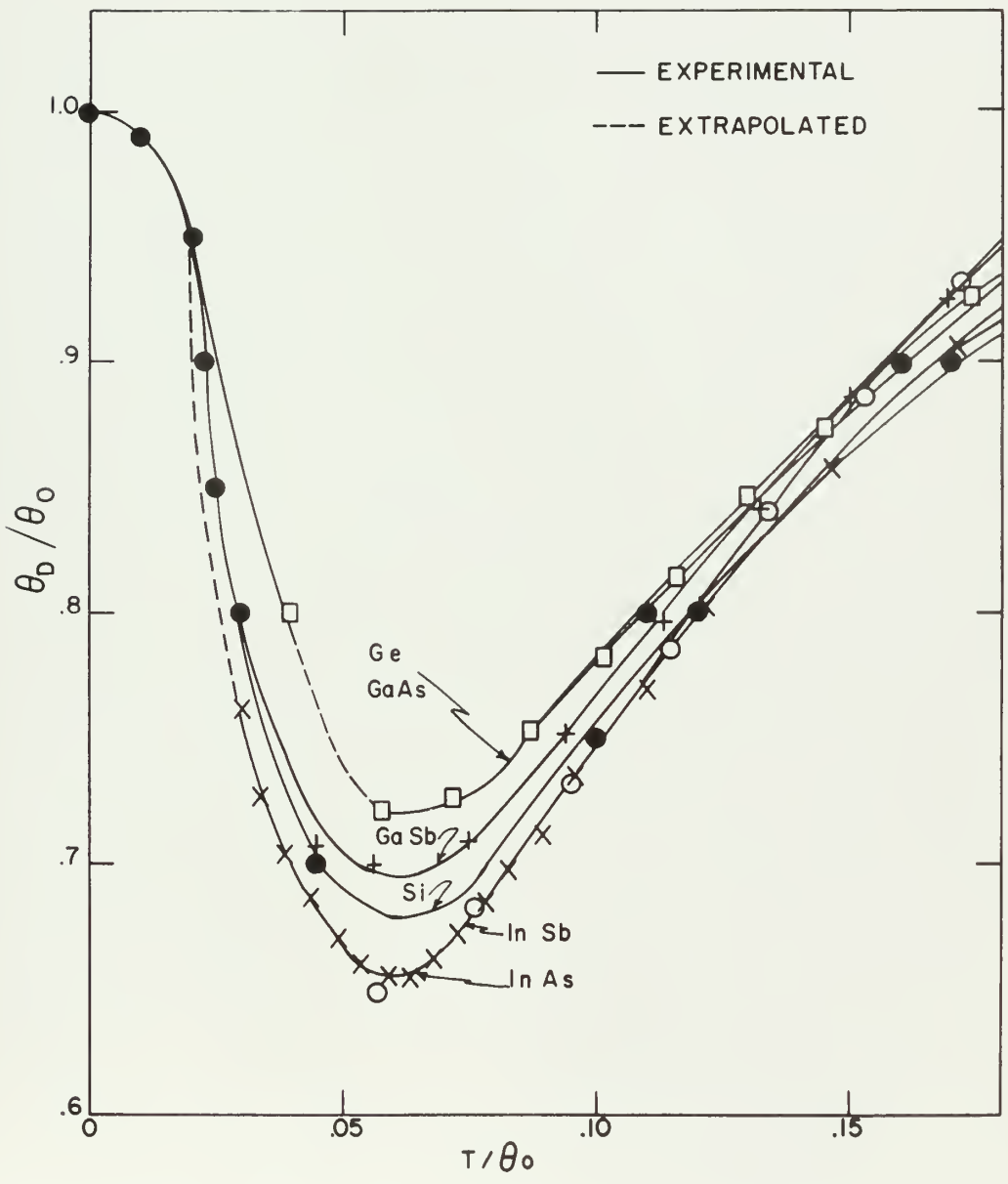
EXPERIMENTAL
EXTRAPOLATED
1.0
.9
.8
.7
.6
θ_D/θ_o
0
.05
.10
.15
T/θ_o
Ge
GaAs
Ga Sb
Si
In Sb
In As

taken from tabulated values of the Debye function. Smoothed values of γ_T are given in Table 2, while a reduced plot of the γ's (γ/γ_o versus T/θ_o) is given in Figure 19.

Figure 19. Reduced γ_T vs. T plot, with γ_o and θ_o as given in Tables 2 and 3

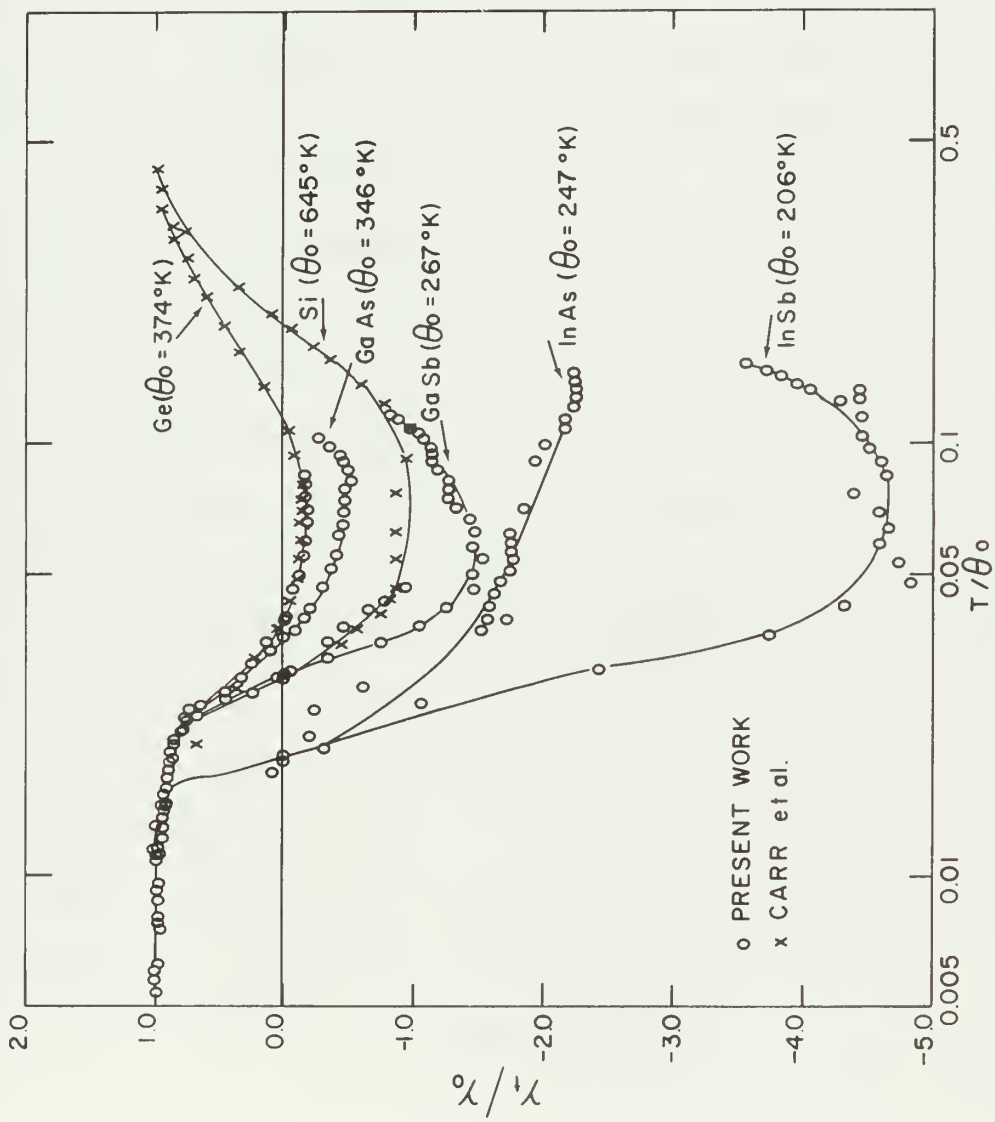
Ge(θ_o = 374°K)
Si (θ_o = 645°K)
Ga As (θ_o = 346°K)
Ga Sb (θ_o = 267°K)
In As (θ_o = 247°K)
In Sb (θ_o = 206°K)
o PRESENT WORK
x CARR et al.
χ_1/χ_o
T/θ_o
2.0
1.0
0.0
-1.0
-2.0
-3.0
-4.0
-5.0
0.005
0.01
0.05
0.1
0.5

DISCUSSION OF RESULTS

The results of this experiment confirm the existence of a low temperature region of positive thermal expansion for the materials measured. The general behavior for all these materials is similar to that shown for Ge in Figure 20. A relatively small positive thermal expansion at very low temperatures is followed by a region of relatively large negative thermal expansion and then by a region of positive thermal expansion for $T/\theta_o > 0.2$.

The thermal expansion coefficient, α, has been shown to be proportional to T^3 at the lowest temperatures ($T/\theta_o < 0.015$) as would be expected from the Debye model. However, the heat capacities of neither Ge nor Si obey a T^3 law even down to $T/\theta_o < 0.01$ and this factor has been used in the extrapolation on Figure 18. Hence, γ_T must increase constantly toward γ_o as the temperature decreases from $T/\theta_o < 0.015$. The deviation of heat capacity from a T^3 behavior is only a few percent for $T/\theta_o \leq 0.01$, so the variation in γ_T for Si below 6^oK is less than the experimental error (about 2%). However, a definite decrease in γ_T can be observed in all cases before the $\alpha = \alpha_o T^3$ region has been passed (see Figure 19). The variation in shape with θ_o for the various reduced γ versus T curves can be seen in Figure 19. There appears to be a definite correlation with the obvious exception of Si.

Sheard (45), Daniels (20), and Collins (46) all have predicted γ_o^{el}'s for Ge and Si using the pressure dependence of the elastic constants for these materials. For Ge, γ_o^{el} is 0.50 and for Si, γ_o^{el} is 0.25, the calculation being based on the low temperature elastic constant vs. pressure data of McSkimmin (21) which is shown in Table 3. These calculations disagree with the values for Ge ($\gamma_o = 0.66$) and Si ($\gamma_o = 0.44$) obtained in

Figure 20. Temperature dependence of the thermal expansion coefficient of Ge

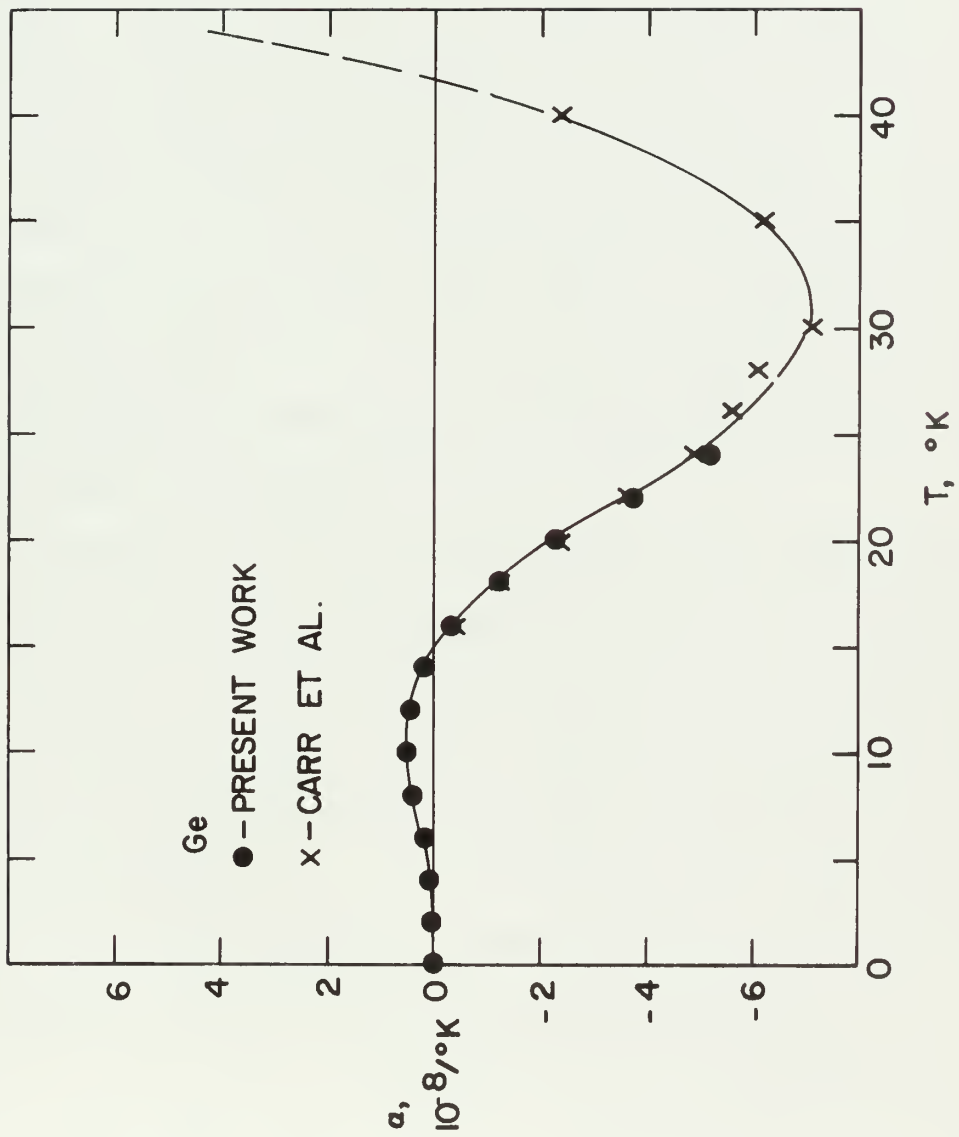
Ge
● – PRESENT WORK
x – CARR ET AL.
a, 10⁻⁸/°K
T, °K
6
4
2
0
-2
-4
-6
0
10
20
30
40

this experiment. At very low temperatures these materials should behave as continuum solids so the calculations should apply as well as for other solids (46). These discrepancies are well outside of the expected errors in both the high pressure elastic constant data and the low temperature thermal expansion data, so no reason can be given at present for these discrepancies. The data of Carr et al. (19) agree with the data of this experiment within the combined experimental errors (see Figures 12 and 13) making an error of 30 to 50 percent in the thermal expansion data unlikely.

Another source of error in this experiment could involve an electronic or carrier contribution to the elastic constants as described by Keyes (24). But, as can be seen in Table 1 the carrier concentrations of our samples (with the exception of GaAs) are all 10^{17} atoms/cm^3 or less and impurity effects should be negligible.

In an attempt to determine the existence of correlations between the physical features of the thermal expansions of the various materials in this experiment, a tabulation of these features (as defined in Figure 21) is shown in Table 4. These features include T_L and T_H, the two temperatures at which $\alpha = 0$; T_D, the temperature at which the expansion first deviates from a T^4 behavior; and T_{min}, the temperature at which the minimum thermal expansion coefficient occured. Also are listed ΔL_{max}, the height of the low temperature positive thermal expansion normalized to a 10 cm sample length; γ_{min}, the value of the minimum γ_T; γ_o, the low temperature limit of γ_T; and α_o the coefficient of T^3 in the expression for α ($=\alpha_o T^3$) below T_D.

It can be seen from Table 4 that with the exception of Si there appears to be a definite correlation between these physical features of the thermal expansions and the value of θ_o. T_{min} (which is roughly constant) is

Figure 21. General behavior of the thermal expansion for a typical tetrahedrally bonded solid with physical features denoted

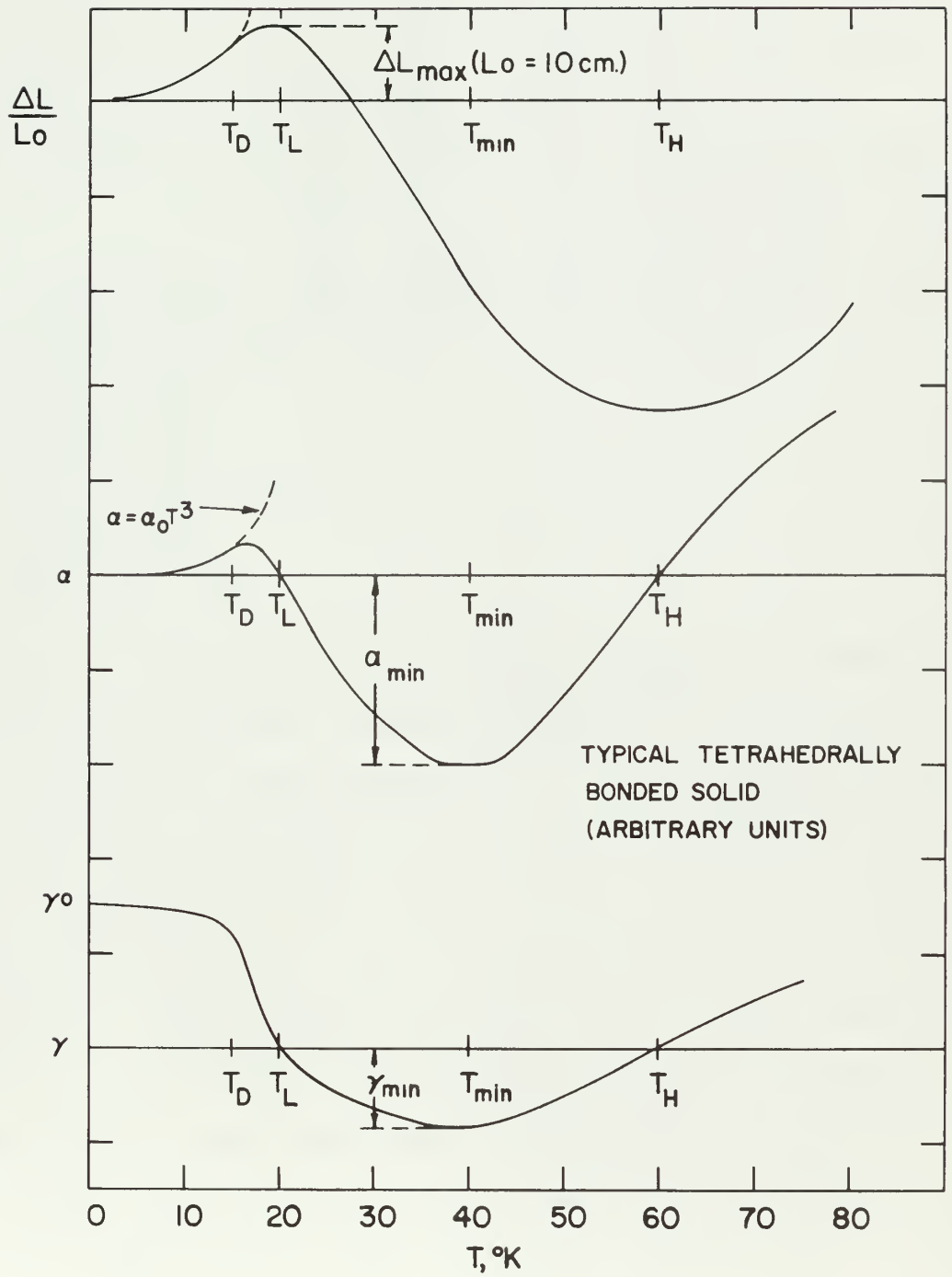
ΔL/Lo
ΔL max (Lo = 10 cm.)
T_D
T_L
T_min
T_H
α = α_0 T^3
α
α min
TYPICAL TETRAHEDRALLY
BONDED SOLID
(ARBITRARY UNITS)
γ_0
γ
γ_min
0
10
20
30
40
50
60
70
80
T, °K

Table 4. Physical features of the thermal expansions

		Si	Ge	GaAs	GaSb	InAs	InSb
T_L	^oK	18.6	14.7	12.2	7.7	4.6	3.9
T_H	^oK	120[a]	48[b]	55[c]	52[d]		67[e]
T_o	^oK	15.9	9.2	8.0	6.6	3.5	3.0
T_{min}	^oK	75[f]	32	31.2	28	35	30
ΔL_{max}	$\AA$	17.9	32.5	22.4	6.65	0.79	0.60
α_{min}	$10^{-7}/^oK$	-5	-0.95	-2.63	-4.40	-15.3	-18.3
γ_{min}		-0.43[f]	-0.11	-0.29	-0.45	-0.73	-0.89
γ_o		0.44	0.66	0.56	0.32	0.33	0.21
α_o	$T^3 \times 10^{-12}$ ^oK	0.88	7.80	8.40	10.7	13.6	16.4

[a] Novikova et al. (13)
[b] Novikova (14)
[c] Novikova (17)
[d] Novikova et al. (18)
[e] Novikova (16)
[f] Carr et al. (19)

an exception. Therefore, a plot of the γ_o's and γ_{min}'s was made as a function of θ_o (see Figure 22). With the exception of Si both the γ_o's and the γ_{min}'s appear to be a linear function of θ_o. If one considers these materials to be members of a "group" (excluding Si) then it may be possible to predict that any member of this "group" which has a value of θ_o below 137 ($\pm$10)^oK will not have a region of positive thermal expansion at very low temperatures. Also, any member which has a value of θ above 405 ($\pm$10)^oK will not have a region of negative thermal expansion. Hence, the value of θ_o for a member of this "group" can be used to obtain both γ_o and γ_{min}. Unfortunately, at the present time there are no criteria for the conditions necessary to become a member of this "group" and the part which Si takes is unknown. It would be valuable to obtain the low temperature thermal expansions of such

Figure 22. The dependence of γ_o and γ_{min} (Figure 21) on θ_o

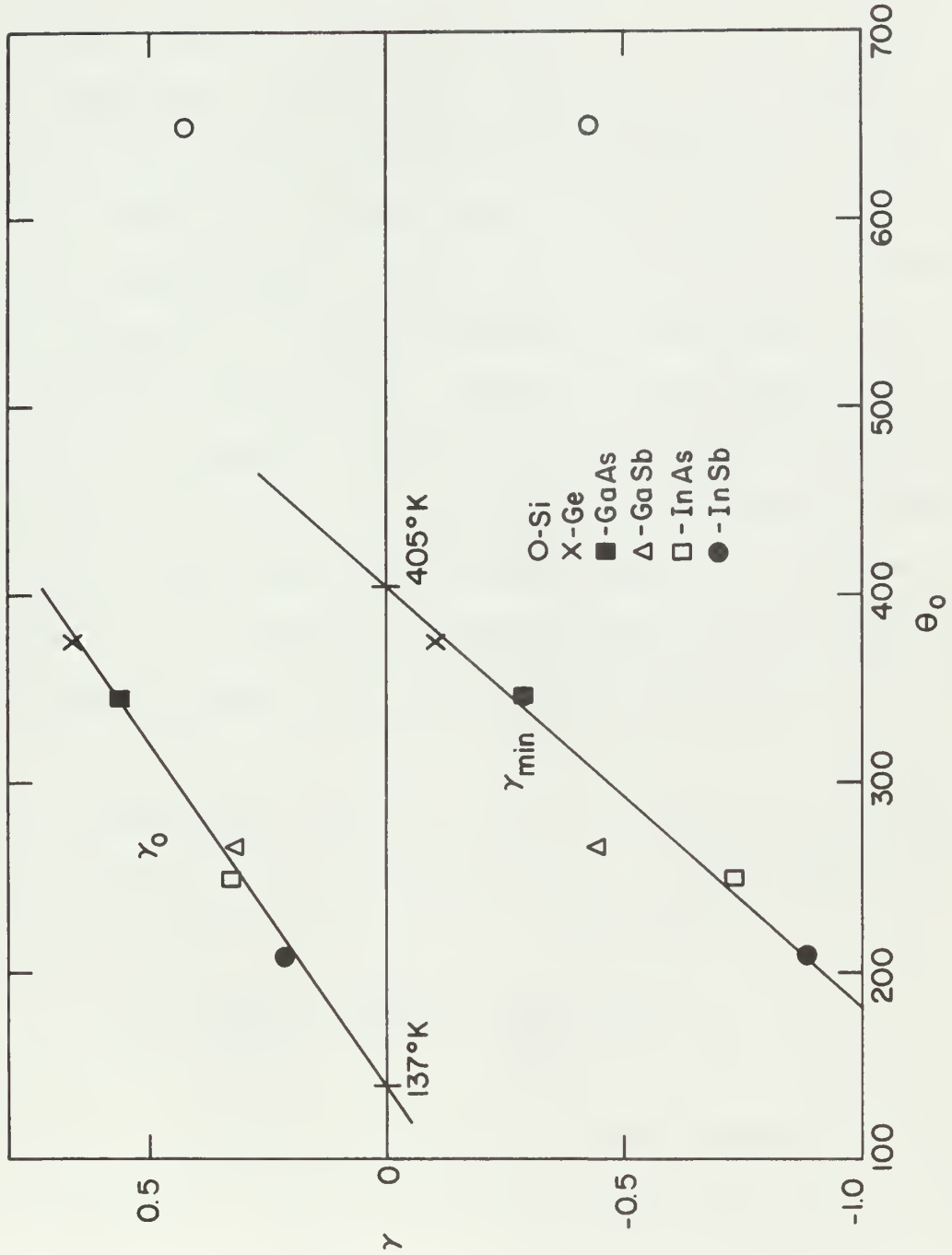
0.5
0
-0.5
-1.0
γ
100
200
300
400
500
600
700
θ₀
137°K
405°K
γ₀
γmin
O-Si
X-Ge
■-GaAs
Δ-GaSb
□-InAs
●-InSb

materials as AlP($\theta_o \simeq 590^oK$), AlAs($\theta \simeq 420^oK$), and CdTe($\theta_o \simeq 140^oK$) to investigate the "anomalous" behavior that Si takes in these correlations and to test the predictions made for a member of the "group". Thermal expansion measurements have been made on CdTe by Novikova (16), but these measurements do not extend to sufficiently low temperatures or are not sufficiently sensitive to test the suggestion that γ_o will be close to zero or even slightly negative in this case. It also would be valuable if more data existed for the pressure dependence of the elastic constants of other tetrahedrally bonded solids. Perhaps the discrepancies involved between the γ_o's so obtained and those of thermal expansion measurements could be resolved. This type of measurement also might show the same type of correlation as has been indicated in this experiment. Also some information on the γ's may be gained from phonon-assisted tunneling under pressure as investigated by Payne (47) as this experiment measures γ_i at the band edges.

The low temperature limit of the Gruneisen constant, γ_o, is given by the volume dependence of θ_o (see equation 33). de Launay (48) has prepared tables for the evaluation of θ_o using the relationship

$$\theta_o^3 = \frac{9N}{4\pi V} \left(\frac{h}{k}\right)^3 \left(\frac{C_{44}}{\rho}\right)^{3/2} \frac{9}{18\sqrt{3}} f(s,t) \quad , \tag{44}$$

where f(s,t) is a relationship between the elastic constants, V is the molar volume, and ρ is the density. Using equation 33, it follows that

$$\gamma_o = - \frac{d \ln\theta_o}{d \ln V}$$

$$= -\frac{1}{2}\frac{d\ \ln C_{44}}{d\ \ln V} - \frac{1}{6} - \frac{1}{3}\frac{d\ \ln f(s,t)}{d\ \ln V} \quad . \tag{45}$$

Daniels (20) computed γ_o for Ge and Si using this relationship and observed that the third terms were small and did not vary much between the two materials. Therefore, since the second term is constant the first term is of primary importance. This term may be expressed as

$$\frac{1}{2}\ \frac{d\ \ln\ C_{44}}{d\ \ln\ V} = -\frac{1}{2}\frac{B_T}{C_{44}}\frac{dC_{44}}{dP} \quad . \tag{46}$$

Since the ratio B_T/C_{44} for the materials measured in this experiment varies from 1.12 (for Ge) to 1.52 (for InAs), the large variation in γ_o (a factor of three) must arise from the pressure dependence of C_{44}. Unfortunately, it is difficult to develop an expression for dC_{44}/dP from first principles and to relate this expression to θ_o. At the present time there is no way to justify theoretically a linear relationship between the γ's and θ_o, or to show why Si differs from the other five materials.

CONCLUSIONS

The results of this experiment have demonstrated the presence of a low temperature region of positive thermal expansion in the materials measured. It seems apparent that all tetrahedrally bonded solids, except possibly those with a very low θ_o, should exhibit the same behavior. The experimental behavior of these solids is understood qualitatively in terms of the pressure dependence of the ω vs. k relationship for the lowest transverse acoustic mode. The pressure dependence of the elastic constants (for Ge and Si) have shown that $\gamma > 0$ for small k while phonon-assisted tunneling experiments have shown that $\gamma < 0$ at the band edge (47). Hence, the shape of this dispersion curve must change appreciably with pressure, while the other phonon branches show "normal" ($\gamma > 0$) behavior.

The band structures of Ge and Si are fairly well understood in basic terms, but the pressure dependence of these bands involves too many unknowns and further theoretical work is necessary. Any theoretical basis for the relationships between γ_o's and γ_{min}'s and θ_o is nonexistent at the present time. Also, the discrepancies between the γ_o's and γ_o^{el}'s for Ge and Si are not understood unless, perhaps, continuum theory is not applicable to the tetrahedrally bonded structures even at low temperatures. The need for further work on the pressure dependences of the elastic constants of these materials is obvious.

To study the thermal expansions of diamond structure materials in more detail would require more sensitivity. The present apparatus has been used close to its maximum sensitivity, and to increase the precision of the experiment it might be worthwhile to consider the use of superconducting

wire in the linear variable differential transformer. With the use of superconducting windings the primary current, and therefore the sensitivity, could be increased by a factor of 100 as the present primary current is limited by the helium boil-off rate in the dewar. Also if the secondary coil were constructed with superconducting wire the matching into the detector-amplifier would be almost unlimited. Unfortunately, at the present two problems exist. First the eddy-current heating produced by the primary current in the sample chamber could be uncontrollable. Second the use of low frequency alternating currents in superconducting wire is not fully understood, and hysteresis losses and locked-in flux are greater than can be tolerated.

LITERATURE CITED

1. Collins, J. G. and White, G. K., Progress in Low Temperature Physics 4, 450 (1964).
2. Andres, K., Cryogenics 2, 93 (1961).
3. Jones, R. V. and Richards, J. C. S., J. Sci. Inst. 36, 90 (1959).
4. White, G. K., Cryogenics 1, 151 (1961).
5. Carr, R. H. and Swenson, C. A., Cryogenics 4, 76 (1964).
6. Fizeau, H., Ann. Phys. 208, 292 (1867).
7. Erfling, H. D., Ann. Phys., Lpz. 41, 467 (1942).
8. Corrucinni, R. J. and Gniewek, J. J., National Bureau of Standards Circular 1 (1961).
9. Adenstedt, H., Ann. Phys., Lpz. 26, 69 (1936).
10. Schuch, A. F. and Laquer, H. L., Phys. Rev. 86 803 (1952)
11. Gibbons, D. F., Phys. Rev. 112, 136 (1958).
12. Blackman, M., Phil. Mag. 3, 831 (1958).
13. Novikova, S. I. and Strelkov, P. G., Fiz. Tverd. Tela 1, 1841 (1959).
14. Novikova, S. I., Fiz. Tverd. Tela 2, 43 (1960).
15. Novikova, S. I., Fiz. Tverd. Tela 2, 1617 (1960).
16. Novikova, S. I., Fiz. Tverd. Tela 2, 2341 (1960).
17. Novikova, S. I., Fiz. Tverd. Tela 3, 178 (1961).
18. Novikova, S. I. and Abrikasor, N. K., Fiz. Tverd. Tela 5, 2138 (1963).
19. Carr, R. H., McCammon, R. D. and White, G. K., Phil. Mag. 12, 157 (1965).
20. Daniels, W. B., Phys. Rev. Letters 8, 3 (1962).
21. McSkimmin, H. J., J. Acoust. Soc. Amer. 30, 314 (1957).
22. Novikova, S. I., Fiz. Tverd. Tela 7, 3331 (1965).
23. Novikova, S. I., Fiz. Tverd. Tela 7, 2493 (1965).

24. Keyes, R. W., IBM Journal Res. Dev. 5, 266 (1961).

25. Daniels, W. B., Int. Conf. of Semiconductor Phys., Exeter Eng., Proc. 1962, 482 (1962).

26. Bienenstock, A., Phil. Mag. 9, 755 (1964).

27. Finnemore, D. K., Ostenson, J. E. and Stromberg, T. F., Rev. Sci. Inst. 36, 1369 (1965).

28. Berman, R. and Mate, C. F., Nature, Lond. 182, 1661 (1958).

29. Rhinehart, W. A. and Mourlam, L., Jr., U. S. Atomic Energy Commission Report IS-821, [Iowa State Univ. of Science and Technology, Ames. Inst. for Atomic Research] 1 (1964).

30. Hedgcock, F. T., Phys. Rev. 6, 1564 (1956).

31. Hannay, N. B., Semiconductors, Reinhold Publishing Corporation, New York (1959).

32. Flubacher, P., Leadbetter, A. J., and Morrison, J. A., Phil. Mag. 4, 273 (1959).

33. Verma, J. K. D., Nag, B. D., and Nair, P. S., Z. Naturforsch. 19a, 1561 (1964).

34. McSkimmin, H. J. and Andreatch, P. Jr., J. Appl. Phys. 35, 2161 (1964).

35. McSkimmin, H. J., J. Appl. Phys. 24, 988 (1953).

36. Garland, C. W. and Park, K. C., J. Appl. Phys. 33, 759 (1962).

37. Einspruch, N. G. and Manning, R. J., J. Acoust. Soc. Amer. 35, 215 (1963).

38. Gerlich, D., J. Appl. Phys. 34, 2915 (1963).

39. Potter, R. F., Phys. Rev. 103, 47 (1956).

40. Aigrain, P. and Balkanski, M., Eds., Selected Constants Relative to Semiconductors, Pergamon Press, London (1961).

41. Giesecke, G. and Pfister, H., Acta Cryst. 11, 369 (1958).

42. Kopperman, J. and Lauder, G., Z. Angew. Phys. 11, 164 (1959).

43. Ohmuro, Y., J. Phys. Soc. Japan 20, 350 (1965).

44. Riesbergen, V., Z. Naturforsch. 180, 141 (1963).

45. Sheard, F. W., Phil. Mag. 3, 1381 (1958).

46. Collins, J. G., Phil. Mag. 8, 323 (1963).

47. Payne, R. T., Phys. Rev. Letters 13, 53 (1964).

48. de Launay, J., Solid State Physics 2, 219 (1958).

ACKNOWLEDGMENTS

I would like to thank Dr. C. A. Swenson for his guidance and interesting discussions and Drs. J. G. Collins, D. K. Finnemore, and H. H. Sample for their helpful discussions. I would also like to thank Mr. K. O. McLean for his kind assistance with both the taking of the data and the use of the computer to analyze the data.

APPENDIX

Experimental Data

These tables contain the data taken in this experiment. The column headings stand for the Au-Fe thermocouple reading (TC), the temperature (T) obtained from our present calibration, and the change in length of the sample (ΔL). These data were obtained by establishing first a base point which corresponds to a fixed value of the heater current I_H, and sample temperature (initially this would be with $I_H = 0$). At this point the thermocouple, TC, and ratio transformer, n, readings would be recorded. The heater current then would be increased slightly (by switching to a different control on the heater current supply), the TC and Δn would be recorded, and then the sample would be returned to the base point. At low temperatures readings would be taken for ΔT's of approximately 0.1 or 0.2 degrees. At intervals of one or two degrees a new base point would be established and the procedure repeated. While taking data between base points values of Δn would be taken with both increasing and decreasing temperature and system checks would be made as described previously. Therefore, all data points are taken as differences from the previous base point. All points were taken at least twice (at lower temperatures they were taken as many as twelve times) and these values were averaged and are shown in order of increasing temperature in these tables. At higher temperatures the same procedure was followed except that base points were taken every 2 degrees or so and the set of points were taken at 0.1 degree intervals.

The low temperature data are shown in these tables with the base points

underlined and the groups separated by a space. The base points of the high temperature data have a line both over and under the value and a space is also provided between groups. At lower temperatures the ΔL_i's between each point are summed giving a continuous ΔL as the temperature increases. At higher temperatures only the base ΔL_i's are summed since the ΔL_i's within a set are used only to determine α. In some instances a base point at higher temperatures was not taken and in these cases the base ΔL is indicated by a dash. Since this was done many times for InAs (the first sample measured) an additional set of data was taken, with only $1.89^{\circ}K$ as a base point, up to $36^{\circ}K$.

SILICON

TC μV	T °K	ΔL °A	TC μV	T °K	ΔL °A
		Lo = 13.65 cm			
0.0	1.89	0.00	120.3	11.71	5.62
4.0	2.30	0.01	125.3	12.07	6.41
8.0	2.71	0.01	130.3	12.42	7.32
12.0	3.10	0.01	135.3	12.79	8.14
16.0	3.49	0.04	140.3	13.15	8.96
20.0	3.86	0.04	145.3	13.51	10.00
24.0	4.23	0.09			
28.0	4.58	0.14	150.7	13.90	11.24
			155.7	14.26	12.01
30.0	4.76	0.14	160.7	14.62	13.16
34.0	5.11	0.20	165.7	14.98	14.72
38.0	5.44	0.25	170.7	15.35	16.41
42.0	5.77	0.31	175.7	15.71	17.91
46.0	6.10	0.37			
50.0	6.42	0.48	180.7	16.07	19.13
54.0	6.74	0.59	185.7	16.43	20.26
58.0	7.05	0.71	190.7	16.80	21.02
			195.7	17.17	22.46
60.5	7.24	0.79	200.7	17.53	23.31
64.5	7.55	0.96	205.7	17.90	23.90
68.5	7.85	1.16			
72.5	8.16	1.36	210.6	18.26	24.18
76.5	8.46	1.55	215.6	18.63	24.32
80.5	8.77	1.84	220.6	19.00	24.19
84.5	9.07	2.06	225.6	19.36	23.82
88.5	9.36	2.29	230.6	19.73	23.25
			235.6	20.09	21.84
90.4	9.51	2.57	240.6	20.46	20.82
94.4	9.81	2.80			
98.4	10.10	3.14			
102.4	10.40	3.62			
106.4	10.69	3.93			
110.4	10.98	4.41			
114.4	11.28	4.92			
118.4	11.57	5.37			

263.7	22.12	7.26	291.3	24.07	-24.9
264.7	22.20	-0.73	292.3	24.14	-1.36
265.7	22.27	-1.47	293.3	24.21	-2.71
266.7	22.34	-2.32	294.3	24.27	-4.12
267.7	22.41	-3.11	295.3	24.35	-5.48
268.7	22.48	-3.90	296.3	24.42	-6.95

Silicon Continued

TC μV	T °K	ΔL Å
321.5	26.11	-90.6
322.5	26.18	-2.49
323.5	26.24	-5.03
324.5	26.31	-7.63
325.5	26.38	-10.11
326.5	26.44	-12.71
351.3	28.03	-205
352.3	28.10	-3.73
353.3	28.16	-7.40
354.3	28.22	-11.19
355.3	28.28	-14.92
356.3	28.35	-18.59
381.3	29.86	-372
382.3	29.92	-5.42
383.3	29.98	-10.79
384.3	30.04	-16.22
385.3	30.10	-21.70
386.3	30.16	-27.12

GERMANIUM

TC μV	T °K	ΔL Å	TC μV	T °K	ΔL Å
		Lo = 13.46 cm			
0.0	1.89	0.00	90.4	9.51	20.74
4.0	2.30	0.06	94.4	9.81	22.66
8.0	2.71	0.11	98.4	10.10	24.49
12.0	3.10	0.28	102.4	10.40	25.74
16.0	3.49	0.37	106.4	10.70	27.63
20.0	3.86	0.57	110.4	10.99	29.52
24.0	4.23	0.79	114.4	11.28	31.84
28.0	4.58	1.13	118.4	11.57	33.28
30.1	4.76	1.36	121.1	11.76	33.76
34.1	5.11	1.75	125.1	12.05	34.97
38.1	5.44	2.26	129.1	12.34	37.06
42.1	5.78	2.94	133.1	12.63	38.34
46.1	6.10	3.62	137.1	12.92	39.69
50.1	6.42	4.38	141.1	13.21	40.77
54.1	6.74	5.25	145.1	13.49	41.92
58.1	7.05	6.61	149.1	13.78	42.54
60.2	7.22	7.29	151.3	13.94	42.80
64.2	7.53	8.36	156.3	14.30	43.11
68.2	7.84	9.55	161.3	14.66	43.25
72.2	8.14	11.87	166.3	15.02	43.22
76.2	8.45	13.50	171.3	15.39	42.57
80.2	8.75	15.23	176.3	15.75	41.90
84.2	9.05	17.54			
88.2	9.35	19.80	180.9	16.09	40.79
			185.9	16.45	39.07
			190.9	16.82	38.17
			195.9	17.19	35.28
			200.9	17.55	32.32
			205.9	17.92	26.58
			210.9	18.29	16.92
		Lo = 6.99 cm			
0.0	1.89	0.00	121.1	11.76	17.56
15.0	3.39	0.17	136.1	12.84	20.44
30.1	4.76	0.72	151.3	13.94	22.25
45.1	6.02	1.74	166.3	15.03	22.57
60.3	7.23	3.66	181.0	16.10	21.17
75.3	8.38	6.60	196.0	17.19	18.35
90.4	9.52	10.78	211.0	18.29	8.69
105.4	10.62	14.11			

Germanium Continued

TC μV	T °K	ΔL °Å	TC μV	T °K	ΔL °Å
207.3	18.03	8.60	317.1	25.82	-200
208.3	18.10	-0.73	318.1	25.89	-3.11
209.3	18.17	-1.53	319.1	25.95	-6.21
210.3	18.25	-2.20	320.1	26.02	-9.32
211.3	18.32	-2.94	321.1	26.08	-12.49
212.3	18.39	-3.67	322.1	26.15	-15.65
237.2	20.21	-17.7	347.0	27.76	-301
238.2	20.29	-1.24	348.0	27.82	-3.5
239.2	20.36	-2.60	349.0	27.89	-7.1
240.2	20.43	-3.90	350.0	27.95	-10.7
241.2	20.50	-5.25	351.0	28.01	-14.4
242.2	20.58	-6.61	352.0	28.08	-18.0
263.7	22.12	-59.3	376.9	29.61	-412
264.7	22.19	-1.92	377.9	29.67	-3.8
265.7	22.26	-3.90	378.9	29.72	-7.7
266.7	22.34	-5.88	379.9	29.78	-11.7
267.7	22.41	-7.85	380.9	29.84	-15.7
268.7	22.48	-9.89	381.9	29.90	-19.5
289.8	23.96	-118.9	410.0	31.52	-518
290.8	24.03	-2.60	411.0	31.58	-3.7
291.8	24.10	-5.31	412.0	31.64	-7.5
292.8	24.17	-7.97	413.0	31.69	-11.2
293.8	24.24	-10.68	414.0	31.75	-15.0
294.8	24.31	-13.39	415.0	31.80	-18.7

GaAs

L_o = 8.26 cm

Run I

TC μV	T °K	ΔL Å
0.0	1.89	0.00
2.0	2.10	0.00
4.0	2.30	0.00
6.0	2.51	0.03
8.0	2.71	0.06
10.0	2.91	0.11
12.0	3.10	0.14
14.0	3.30	0.17
16.0	3.49	0.20
18.0	3.68	0.28
20.0	3.86	0.31
22.0	4.05	0.40
24.0	4.23	0.48
26.0	4.41	0.57
28.0	4.58	0.65
30.1	4.77	0.79
32.1	4.94	0.96
34.1	5.11	1.05
36.1	5.28	1.27
38.1	5.45	1.41
40.4	5.64	1.64
42.4	5.80	1.84
44.4	5.96	2.06
46.4	6.13	2.35
48.4	6.29	2.66
50.4	6.45	2.97
52.4	6.61	3.28
54.4	6.77	3.64
56.4	6.92	4.04
58.4	7.08	4.44
60.4	7.23	4.89
62.4	7.39	5.25
64.4	7.54	5.71
66.4	7.70	6.13
68.4	7.85	6.64
70.5	8.01	7.01
72.5	8.16	7.43
74.5	8.31	7.91
76.5	8.47	8.45
78.5	8.62	8.93
80.6	8.79	9.38
82.6	8.93	9.89
84.6	9.08	10.34
86.6	9.23	10.88
88.6	9.38	11.47
90.7	9.53	12.09
92.7	9.68	12.57
94.7	9.83	13.05
96.7	9.98	13.53
98.7	10.13	14.10
100.6	10.26	14.66
102.6	10.41	15.17
104.6	10.56	15.65
106.6	10.70	16.13
108.6	10.85	16.55
111.0	11.03	17.09
113.0	11.18	17.46
115.0	11.32	17.71
117.0	11.47	18.02
119.0	11.61	18.22
121.4	11.79	18.36
123.4	11.93	18.36
125.4	12.08	18.39
127.4	12.22	18.42
129.4	12.37	18.39
131.3	12.50	18.36
133.3	12.64	18.22
135.3	12.79	17.95
137.3	12.93	17.54
139.3	13.08	16.92
141.4	13.23	16.13
143.4	13.38	15.23
145.4	13.52	14.35
147.4	13.66	13.48
149.4	13.81	12.57

GaAs Continued

TC μV	T °K	ΔL Å
151.6	13.96	11.61
153.6	14.11	10.48
155.6	14.25	9.13
157.6	14.39	7.71
159.6	14.54	6.30
177.7	15.86	-26.9
178.7	15.93	-1.47
179.7	16.00	-3.05
180.7	16.08	-4.58
181.7	16.15	-6.10
182.7	16.22	-7.63
197.7	17.32	-76.3
198.7	17.39	-2.77
199.7	17.46	-5.59
200.7	17.54	-8.42
201.7	17.61	-10.68
202.7	17.68	-13.39
218.3	18.83	-155.2
219.3	18.90	-3.67
220.3	18.97	-7.51
221.3	19.05	-11.13
222.3	19.12	-14.86
223.3	19.19	-18.70
244.5	20.74	-290.3
245.5	20.81	-5.4
246.5	20.89	-10.9
247.5	20.96	-16.3
248.5	21.03	-21.8
249.5	21.10	-27.2
243.4	20.66	-241.8
244.4	20.74	-5.4
245.4	20.81	-10.9
246.4	20.88	-16.3
247.4	20.95	-21.8
248.4	21.03	-27.2
265.0	22.22	-394.5
266.0	22.29	-6.8
267.0	22.36	-13.3
268.0	22.43	-20.1
269.0	22.50	-26.8
270.0	22.57	-33.3
286.4	23.73	-581.5
287.4	23.80	-7.9
288.4	23.87	-15.8
289.4	23.94	-24.9
290.4	24.01	-32.8
291.4	24.08	-41.2
311.9	25.48	-843.1
312.9	25.54	-9.0
313.9	25.61	-18.6
314.9	25.68	-28.3
315.9	25.74	-37.9
316.9	25.81	-47.5
334.6	26.97	-1131.2
335.6	27.03	-10.2
336.6	27.10	-20.9
337.6	27.16	-31.6
338.6	27.23	-41.8
339.6	27.29	-53.1
351.0	28.02	-1408.1
352.0	28.08	-11.9
353.0	28.14	-23.7
354.0	28.20	-36.2
355.0	28.27	-48.0
356.0	28.33	-59.9

GaAs Continued

TC μV	T °K	ΔL °A
377.7	29.65	-1779.9
378.7	29.71	-12.4
379.7	29.77	-24.9
380.7	29.83	-37.3
381.7	29.89	-50.3
382.7	29.95	-62.7
403.0	31.13	-2152.2
404.0	31.18	-11.9
405.0	31.24	-24.3
406.0	31.30	-37.3
407.0	31.35	-49.7
408.0	31.41	-61.0
426.4	32.43	-2472.0
427.4	32.49	-11.3
428.4	32.54	-22.0
429.4	32.60	-33.3
430.4	32.65	-44.6
431.4	32.70	-55.9

TC μV	T °K	ΔL °A
450.5	33.72	-2790
451.5	33.77	-10.2
452.5	33.82	-19.8
453.5	33.87	-29.4
454.5	33.92	-38.4
455.5	33.97	-48.0
475.5	34.98	-3060
476.5	35.03	-7.9
477.5	35.08	-15.8
478.5	35.13	-23.2
479.5	35.18	-31.6
480.5	35.22	-40.1

Run II

0.0	1.90	0.00
4.0	2.31	0.03
8.0	2.72	0.06
12.0	3.11	0.14
16.0	3.49	0.20
20.0	3.86	0.31
24.0	4.22	0.51
28.0	4.57	0.65
30.1	4.76	0.82
34.1	5.10	1.07
38.1	5.44	1.44
42.1	5.77	1.86
46.1	6.10	2.37
50.1	6.43	2.94
54.1	6.74	3.67
58.1	7.06	4.41
60.1	7.22	4.80
244.5	20.74	-
245.5	20.81	-5.5
246.5	20.89	-10.8
247.5	20.96	-16.2
248.5	21.03	-21.7
249.5	21.10	-27.1
287.4	23.80	-
288.4	23.87	-8.5
289.4	23.94	-16.4
290.4	24.01	-24.9
291.4	24.08	-32.8
292.4	24.15	-41.2
335.4	27.02	-
336.4	27.08	-10.7
337.4	27.15	-20.9
338.4	27.21	-31.6
339.4	27.28	-41.8
340.4	27.34	-52.5
378.1	29.68	-
379.1	29.74	-12.4
380.1	29.80	-24.9
381.1	29.86	-37.9
382.1	29.92	-50.3
383.1	29.97	-62.7

GaSb

Lo = 10.06 cm

TC μV	T °K	ΔL °A	TC μV	T °K	ΔL °A
0.0	1.89	0.0	49.9	6.41	4.41
2.0	2.10	0.02	51.9	6.57	4.92
4.0	2.30	0.06	53.9	6.72	5.34
6.0	2.51	0.09	55.9	6.88	5.74
8.0	2.71	0.14	57.9	7.04	6.07
10.0	2.91	0.18			
12.0	3.10	0.23	59.9	7.19	6.38
14.0	3.30	0.28	61.9	7.35	6.53
16.0	3.49	0.34	63.9	7.51	6.64
18.0	3.68	0.54	65.9	7.66	6.64
20.0	3.86	0.62	67.9	7.81	6.64
22.0	4.05	0.72			
24.0	4.23	0.85	69.9	7.97	6.61
26.0	4.41	0.98	71.9	8.12	6.36
28.0	4.58	1.19	73.9	8.27	5.74
			75.9	8.42	5.09
30.0	4.76	1.47	77.9	8.57	4.24
32.0	4.93	1.64			
34.0	5.10	1.81	79.7	8.72	3.25
36.0	5.27	2.06	81.7	8.87	2.03
38.0	5.44	2.29	83.7	9.02	0.31
			85.7	9.17	-1.67
39.9	5.60	2.63	87.7	9.32	-4.12
41.9	5.77	2.85	89.7	9.46	-6.64
43.9	5.93	3.22			
45.9	6.09	3.64			
47.9	6.25	4.10			

94.6	9.82	-22.5	124.8	12.02	-155.4
95.6	9.90	-1.86	125.8	12.10	-5.54
96.6	9.97	-3.84	126.8	12.17	-11.19
97.6	10.04	-5.71	127.8	12.24	-16.89
98.6	10.12	-7.63	128.8	12.31	-22.43
99.6	10.19	-9.66	129.8	12.38	-27.91
109.7	10.93	-68.3	139.2	13.07	-278.2
110.7	11.00	-3.28	140.2	13.14	-7.34
111.7	11.08	-6.72	141.2	13.21	-14.69
112.7	11.15	-10.23	142.2	13.29	-21.47
113.7	11.22	-13.23	143.2	13.36	-29.38
114.7	11.29	-17.06	144.2	13.43	-36.72

GaSb Continued

TC μV	T °K	ΔL °A
154.4	14.17	-443.8
155.4	14.24	-10.17
156.4	14.31	-20.34
157.4	14.38	-29.94
158.4	14.46	-40.11
159.4	14.53	-50.28
170.0	15.30	-674.9
171.0	15.37	-11.86
172.0	15.44	-23.73
173.0	15.51	-36.16
174.0	15.59	-48.59
175.0	15.66	-60.45
185.0	16.39	-941.0
186.0	16.47	-14.69
187.0	16.54	-29.94
188.0	16.61	-45.76
189.0	16.69	-60.45
190.0	16.76	-75.14
200.4	17.52	-1281.7
201.4	17.59	-17.51
202.4	17.67	-35.03
203.4	17.74	-53.11
204.4	17.81	-70.62
205.4	17.89	-88.14
214.0	18.51	-1645.3
215.0	18.59	-18.64
216.0	18.66	-37.29
217.0	18.73	-57.06
218.0	18.81	-75.14
219.0	18.88	-93.22
228.8	19.60	-2061.0
229.8	19.67	-20.9
230.8	19.74	-41.2
231.8	19.81	-61.6
232.8	19.89	-81.9
233.8	19.96	-103.4
243.8	20.69	-2517.6
244.8	20.76	-23.2
245.8	20.83	-46.9
246.8	20.90	-71.2
247.8	20.98	-93.8
248.8	21.05	-117.0
258.9	21.78	-3027.8
259.9	21.85	-25.4
260.9	21.92	-50.9
261.9	22.00	-76.3
262.9	22.07	-101.7
263.9	22.14	-127.1
273.6	22.83	-3559.5
274.6	22.90	-25.4
275.6	22.97	-51.4
276.6	23.04	-76.3
277.6	23.11	-101.1
278.6	23.18	-127.7
288.8	23.89	-4125.6
289.8	23.96	-26.0
290.8	24.03	-52.0
291.8	24.10	-78.5
292.8	24.17	-104.5
293.8	24.24	-130.5
303.4	24.90	-4701.4
304.4	24.97	-27.1
305.4	25.03	-54.2
306.4	25.10	-81.9
307.4	25.17	-109.0
308.4	25.24	-136.2
318.4	25.91	-5304.2
319.4	25.98	-28.3
320.4	26.04	-56.5
321.4	26.11	-84.1
322.4	26.17	-112.4
323.4	26.24	-140.7

GaSb Continued

TC μV	T °K	ΔL °A
333.2	26.88	-5908.2
334.2	26.94	-27.7
335.2	27.01	-55.9
336.2	27.07	-84.2
337.2	27.14	-111.9
338.2	27.20	-139.0
348.3	27.84	-6522.9
349.3	27.91	-27.1
350.3	27.97	-55.4
351.3	28.03	-83.6
352.3	28.10	-111.3
353.3	28.16	-138.4
363.3	28.78	-7133.7
364.3	28.84	-26.6
365.3	28.90	-53.1
366.3	28.96	-79.7
367.3	29.02	-105.7
368.3	29.08	-131.6
378.0	29.67	-7709.4
379.0	29.73	-24.9
380.0	29.79	-49.2
381.0	29.85	-74.0
382.0	29.91	-98.9
383.0	29.97	-123.7
393.0	30.55	-8250.1
394.0	30.61	-23.2
395.0	30.67	-46.9
396.0	30.73	-70.6
397.0	30.78	-93.2
398.0	30.84	-117.0

InAs

TC μV	T °K	ΔL Å	TC μV	T °K	ΔL Å
		Lo = 10.01 cm			
0.0	1.89	0.00	20.1	3.87	0.63
2.0	2.10	0.00	22.1	4.06	0.67
4.0	2.30	0.03	24.1	4.24	0.71
6.0	2.51	0.06	26.1	4.42	0.72
8.0	2.71	0.13	28.1	4.59	0.75
10.5	2.95	0.20	29.7	4.73	0.72
12.5	3.15	0.29	31.7	4.90	0.69
14.5	3.34	0.38	33.7	5.07	0.63
16.5	3.53	0.47	35.7	5.24	0.52
18.5	3.72	0.56	37.7	5.41	0.36
496.1	35.98	20850	373.4	29.40	11140
464.3	34.42	17990	354.8	28.25	9710
440.9	33.21	16330	334.6	26.97	8330
417.6	31.95	14500	318.1	25.89	7290
401.1	31.02	13210	302.8	24.85	6420
167.9	15.14	-	39.8	5.58	0.26
168.9	15.22	-19.2	41.8	5.75	-0.14
169.9	15.29	-40.7	43.8	5.91	-0.34
170.9	15.36	-62.2	45.8	6.07	-0.54
171.9	15.43	-83.6	47.8	6.24	-0.76
172.9	15.51	-105.1	49.8	6.40	-0.96
197.7	17.32	-	49.7	6.39	-0.71
198.7	17.39	-30.5	51.7	6.55	-0.54
199.7	17.47	-62.2	53.7	6.71	-1.21
200.7	17.54	-93.8	55.7	6.87	-2.01
201.7	17.61	-124.3	57.7	7.02	-3.02
202.7	17.68	-154.8	59.7	7.18	-4.18
265.9	22.28	-	91.1	9.56	-4.89
266.9	22.36	-51	92.1	9.64	-3.84
267.9	22.43	-102	93.1	9.71	-7.85
268.9	22.50	-154	94.1	9.78	-12.03
269.9	22.57	-205	95.1	9.86	-16.27
270.9	22.64	-257	96.1	9.93	-20.79

InAs Continued

TC μV	T °K	ΔL Å
300.5	24.70	-
301.5	24.77	-59
302.5	24.84	-119
303.5	24.91	-179
304.5	24.97	-238
305.5	25.04	-299
326.4	26.44	-
327.4	26.50	-67
328.4	26.57	-134
329.4	26.63	-202
330.4	26.70	-270
331.4	26.76	-337
353.6	28.18	-
354.6	28.24	-69
355.6	28.30	-139
356.6	28.36	-209
357.6	28.43	-279
358.6	28.49	-353
382.2	29.92	-
383.2	29.98	-73
384.2	30.04	-148
385.2	30.10	-223
386.2	30.16	-298
387.2	30.22	-374
410.6	31.56	-
411.6	31.62	-75
412.6	31.67	-153
413.6	31.73	-232
414.6	31.79	-308
415.6	31.84	-388
438.2	33.07	-
439.2	33.12	-79
440.2	33.18	-157
441.2	33.23	-237
442.2	33.28	-318
443.2	33.33	-397

TC μV	T °K	ΔL Å
467.0	34.56	-
468.0	34.61	-76
469.0	34.66	-153
470.0	34.71	-229
471.0	34.76	-306
472.0	34.81	-382
495.0	35.93	-
496.0	35.98	-72
497.0	36.03	-148
498.0	36.08	-221
499.0	36.13	-294
500.0	36.18	-368
81.7	8.86	-34.5
82.7	8.94	-2.0
83.7	9.01	-4.8
84.7	9.09	-7.9
85.7	9.16	-11.2
86.7	9.24	-14.9
87.7	9.31	-18.5
90.8	9.54	-80.1
91.8	9.61	-3.5
92.8	9.69	-7.7
93.8	9.76	-12.4
94.8	9.84	-17.2
101.3	10.31	-146.1
102.3	10.39	-5.0
103.3	10.46	-10.3
104.3	10.53	-15.9
105.3	10.61	-21.7
106.3	10.68	-27.5
110.7	11.00	-228
111.7	11.08	-6.1
112.7	11.15	-12.7
113.7	11.22	-19.4
114.7	11.29	-26.7
115.7	11.37	-34.2

InAs Continued

TC μV	T °K	ΔL °A	TC μV	T °K	ΔL °A
120.5	11.71	-333	149.5	13.81	-849
121.5	11.79	-7.8	150.5	13.89	-15.3
122.5	11.86	-16.2	151.5	13.96	-31.1
123.5	11.93	-25.4	152.5	14.03	-46.9
124.5	12.00	-34.9	153.5	14.10	-63.8
125.5	12.08	-44.4	154.5	14.17	-81.9
130.2	12.42	-468	159.1	14.51	-1091
131.2	12.49	-10.2	160.1	14.58	-17.5
132.2	12.56	-21.5	161.1	14.65	-35.6
133.2	12.63	-32.8	162.1	14.73	-54.8
134.2	12.71	-44.1	163.1	14.80	-74.6
135.2	12.78	-56.5	164.1	14.87	-93.8
139.8	13.11	-639	168.6	15.20	-1368
140.8	13.18	-13.0	169.6	15.27	-19.2
141.8	13.25	-26.6	170.6	15.34	-39.6
142.8	13.32	-40.1	171.6	15.42	-61.0
143.8	13.40	-54.8	172.6	15.49	-82.5
144.8	13.47	-70.1	173.6	15.56	-104.0

InSb

TC μV	T °K	ΔL Å	TC μV	T °K	ΔL Å
		Lo = 10.12 cm			
0.0	1.89	0.00	20.0	3.86	0.54
2.0	2.10	0.02	22.0	4.04	0.54
4.0	2.30	0.07	24.0	4.23	0.50
6.0	2.51	0.12	26.0	4.40	0.42
8.0	2.71	0.17	28.0	4.58	0.29
10.0	2.91	0.25	30.1	4.76	0.18
12.0	3.10	0.31	32.1	4.93	-0.05
14.0	3.30	0.41	34.1	5.10	-0.42
16.0	3.49	0.50	36.1	5.27	-1.26
18.0	3.68	0.52	38.1	5.44	-2.36
			40.1	5.61	-3.72
45.2	6.03	-19.54	108.8	10.86	-841
46.2	6.11	-1.53	109.8	10.93	-24
47.2	6.19	-3.22	110.8	11.01	-49
48.2	6.27	-4.92	111.8	11.08	-74
49.2	6.35	-6.78	112.8	11.15	-100
50.2	6.43	-8.53	113.8	11.22	-126
61.7	7.34	-67.6	125.2	12.06	-1432
62.7	7.42	-5.3	126.2	12.13	-31
63.7	7.49	-10.7	127.2	12.20	-64
64.7	7.57	-15.1	128.2	12.27	-93
65.7	7.65	-20.5	129.2	12.34	-132
66.7	7.73	-27.2	130.2	12.42	-167
77.8	8.57	-206	140.1	13.13	-2154
78.8	8.65	-10.2	141.1	13.20	-43
79.8	8.72	-20.3	142.1	13.27	-86
80.8	8.80	-31.1	143.1	13.35	-129
81.8	8.88	-41.2	144.1	13.42	-173
82.8	8.95	-51.4	145.1	13.49	-217
93.7	9.75	-455	155.8	14.27	-3253
94.7	9.83	-16.9	156.8	14.34	-51
95.7	9.90	-33.9	157.8	14.41	-102
96.7	9.97	-52.0	158.8	14.49	-154
97.7	10.05	-70.6	159.8	14.56	-206
98.7	10.12	-89.8	160.8	14.63	-258

InSb Continued

TC μV	T °K	ΔL Å
176.0	15.73	-4630
177.0	15.81	-60
178.0	15.88	-121
179.0	15.95	-181
180.0	16.03	-242
181.0	16.10	-303
198.2	17.35	-6460
199.2	17.43	-77
200.2	17.50	-154
201.2	17.57	-231
202.2	17.65	-307
203.2	17.72	-385
216.9	18.72	-8320
217.9	18.80	-86
218.9	18.87	-173
219.9	18.94	-259
220.9	19.02	-346
221.9	19.09	-433
235.5	20.08	-10390
236.5	20.15	-93
237.5	20.23	-185
238.5	20.30	-278
239.5	20.37	-371
240.5	20.45	-463
252.9	21.35	-12490
253.9	21.42	-99
254.9	21.49	-200
255.9	21.57	-299
256.9	21.64	-400
257.9	21.71	-499
288.2	23.85	-17240
289.2	23.92	-113
290.2	23.99	-226
291.2	24.06	-339
292.2	24.13	-453
293.2	24.20	-566

TC μV	T °K	ΔL Å
304.7	24.99	-19090
305.7	25.05	-116
306.7	25.12	-233
307.7	25.19	-349
308.7	25.26	-466
309.7	25.32	-581
322.1	26.15	-21700
323.1	26.22	-116
324.1	26.28	-234
325.1	26.35	-351
326.1	26.41	-468
327.1	26.48	-586
339.6	27.29	-24360
340.6	27.36	-116
341.6	27.42	-233
342.6	27.48	-349
343.6	27.55	-466
344.6	27.61	-582
355.6	28.30	-26900
356.6	28.37	-113
357.6	28.43	-226
358.6	28.49	-339
359.6	28.55	-452
360.6	28.61	-566
371.1	29.25	-29340
372.1	29.31	-111
373.1	29.38	-221
374.1	29.44	-332
375.1	29.50	-442
376.1	29.56	-553
386.4	30.17	-31700
387.4	30.23	-103
388.4	30.28	-217
389.4	30.34	-325
390.4	30.40	-434
391.4	30.46	-542
402.4	31.10	-34000
403.4	31.15	-104
404.4	31.21	-208
405.4	31.27	-312
406.4	31.32	-416
407.4	31.38	-521